

# ZEROSIAM: AN EFFICIENT SIAMESE FOR TEST-TIME ENTROPY OPTIMIZATION WITHOUT COLLAPSE

Guohao Chen<sup>1\*</sup>, Shuaicheng Niu<sup>1\*</sup>, Deyu Chen<sup>2</sup>, Jiahao Yang<sup>2</sup>, Zitian Zhang<sup>2</sup>

Mingkui Tan<sup>2</sup>, Pengcheng Wu<sup>1</sup>, Zhiqi Shen<sup>1†</sup>

{guohao.chen, shuaicheng.niu, zqshen}@ntu.edu.sg

Nanyang Technological University<sup>1</sup> South China University of Technology<sup>2</sup>

## ABSTRACT

Test-time entropy minimization helps adapt a model to novel environments and incentivize its reasoning capability, unleashing the model’s potential during inference by allowing it to evolve and improve in real-time using its own predictions, achieving promising performance. However, pure entropy minimization can favor non-generalizable shortcuts, such as inflating the logit norm and driving all predictions to a dominant class to reduce entropy, risking collapsed solutions (*e.g.*, constant one-hot outputs) that trivially minimize the objective without meaningful learning. In this paper, we introduce ZeroSiam, an efficient asymmetric Siamese architecture tailored for test-time entropy minimization. ZeroSiam prevents collapse through asymmetric divergence alignment, which is efficiently achieved by a learnable predictor and a stop-gradient operator before the classifier. We provide empirical and theoretical evidence that ZeroSiam not only prevents collapse solutions, but also absorbs and regularizes biased learning signals, enhancing performance even when no collapse occurs. Despite its simplicity, extensive results show that ZeroSiam performs more stably over prior methods using negligible overhead, demonstrating efficacy on both vision adaptation and large language model reasoning tasks across challenging test scenarios and diverse models, including tiny models that are particularly collapse-prone.

## 1 INTRODUCTION

Entropy measures the uncertainty of a model’s predictions. Since its emergence, entropy optimization has been widely adopted as an auxiliary objective alongside supervised, reinforcement signals, *etc.* To be specific, in semi-supervised learning it enforces low-entropy predictions on unlabeled data to refine decision boundaries (Grandvalet & Bengio, 2004; Lee et al., 2013; Sajjadi et al., 2016); in domain adaptation it mitigates distribution shifts by promoting confident outputs (Jiang & Zhai, 2007; Long et al., 2016; Morerio et al., 2017); and in reinforcement learning it is often maximized to encourage exploration or minimized to ensure deterministic policies (Ziebart et al., 2008; Ahmed et al., 2019), among others, showing its remarkable success in boosting the learning effectiveness.

Of late, **test-time** entropy minimization has attracted growing interest, as it operates purely unsupervised during inference, without relying on any ground-truth supervision. For example, in test-time adaptation (TTA) (Wang et al., 2021; Lee et al., 2024) it encourages confident predictions to mitigate domain shifts on unseen data streams; in large language models, it helps calibrate uncertainty and improve prediction consistency for alignment (Hu et al., 2025a; Jang et al., 2025). These advances highlight the potential of entropy minimization in unleashing model power during inference, enabling adaptation to novel or out-of-distribution domains and moving toward greater intelligence.

However, entropy minimization naturally drives the model to increase the maximum predicted logit, regardless of whether it aligns with the true label. In practice, testing often involves noisy real-world data, domain shifts, or novel environments, where models often tend to be highly sensitive and uncertain, and the predicted maximum class is frequently incorrect. In this sense, minimizing entropy alone does not ensure that the corresponding supervised loss (*e.g.*, cross-entropy) on the

\*Equal contribution. †Corresponding author.

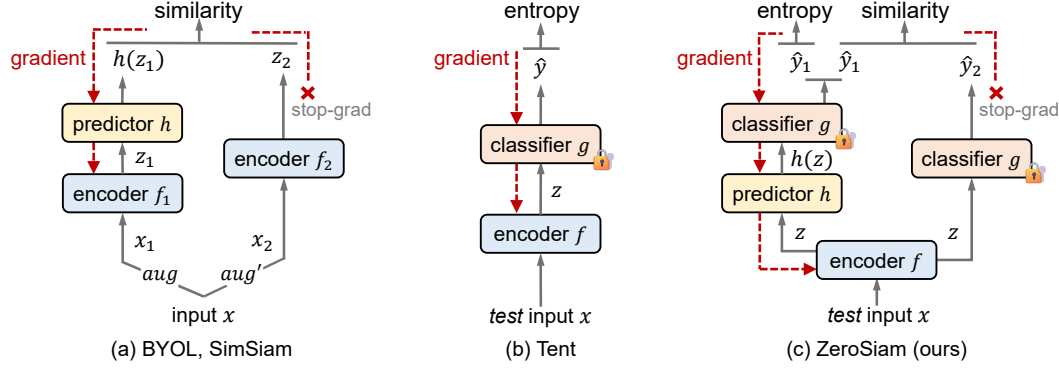


Figure 1: Comparisons on architectures. (a) Alignment-oriented SSL methods (BYOL (Grill et al., 2020), SimSiam (Chen & He, 2021)). (b) Test-time entropy minimization (Tent) (Wang et al., 2021). (c) Our ZeroSiam, which designs a minimal asymmetry for entropy minimization with a lightweight predictor and a stop-gradient branch—without augmentations, extra encoder passes, or teacher models—to substantially enhance learning stability and boost performance while retaining efficiency.

target task is also reduced. Instead, the model can easily exploit a shortcut solution by producing near one-hot outputs for all inputs, which trivially minimizes entropy but fails to capture meaningful predictions, leading to degraded performance. For instance, after TTA, models can deteriorate to predicting all samples to a single class under challenging wild testing scenarios (Niu et al., 2023).

Various TTA methods have been proposed to tackle the above issue, such as filtering unreliable gradients using predefined thresholds (Niu et al., 2022; Lee et al., 2024; Hu et al., 2025a), or mitigating disturbances through optimization of a sharpness-aware loss surface (Niu et al., 2023). However, the use of heuristic thresholds for gradient selection remains problematic, as such thresholds are difficult to define and generalize across domains. In this sense, filtering or suppressing noisy gradients can only be partial, and the model remains exposed to trivial solutions by optimizing with the remaining gradients, for which entropy can still be minimized by collapsing into constant one-hot outputs regardless of the inputs. As a result, it is unavoidable that these methods still risk collapse during deployment, particularly under prolonged or more challenging testing scenarios, as in Tables 2 & 6.

In this paper, we resolve the collapse risk of test-time entropy minimization by drawing inspiration from negative-free self-supervised learning (SSL) (Chen & He, 2021; Zhang et al., 2022a), which seeks to learn meaningful representations by maximizing the similarity between two augmented views of the same image. Negative-free SSL introduces an asymmetric structure to prevent the *two branches* from collapsing toward the same constant, resolving collapse from the architecture design. However, asymmetric structure is originally developed for representation learning, and naively applying asymmetry to our context is infeasible or inferior, as: 1) test-time entropy minimization typically has only one prediction branch and optimizes entropy instead of similarity; 2) traditional Siamese design requires extra backbone passes, which impairs efficiency for our test-time learning.

Therefore, we design ZeroSiam, an efficient asymmetric Siamese architecture tailored for test-time entropy minimization, using zero augmentations and extra backbone passes. To embed asymmetry within a single backbone pass, ZeroSiam decouples a prediction into two asymmetric outputs based on the same feature: an online branch with a learnable predictor and a target branch with stop-gradient. As shown in Figure 1, we minimize entropy on the online branch to learn discriminative features, while performing asymmetric predictor–target alignment to prevent collapsed constant solutions. We investigate ZeroSiam’s behaviors empirically and theoretically during TTA in Section 3.2, demonstrating that our architecture avoids collapse and is also meaningful in absorbing and regularizing biased learning signals at testing, which improves the performance of entropy optimization even when no collapse occurs. ZeroSiam achieves stable and effective entropy minimization using only a single predictor, introducing negligible overhead (see Table 1). Despite its simplicity, ZeroSiam yields superior robustness compared to prior methods across diverse architectures and a wide range of test scenarios, *e.g.*, adapting reliably even with *incorrect* pseudo labels (see Table 6).

**Main Novelty and Contributions:** 1) We propose ZeroSiam, a simple yet effective asymmetric architecture for test-time entropy minimization without collapse, while requiring zero augmentations, no extra backbone passes, and no teacher models to achieve efficient online deployment. 2) We pro-

vide complementary empirical and theoretical insights into ZeroSiam’s behaviors (c.f. Section 3.2), demonstrating that ZeroSiam also helps absorb and regulate non-generalizable biased learning signals at testing, which enhances test-time learning performance even when no collapse occurs. 3) Extensive experiments on both language and vision tasks across both transformer and CNN models with varying sizes and a wide range of challenging test scenarios verify our efficacy.

## 2 PRELIMINARY AND PROBLEM STATEMENT

We briefly revisit test-time entropy minimization in this section for the convenience of our method presentation and put detailed related work discussions into Appendix A due to page limits.

**Test-Time Entropy Minimization** Formally, given any model with its encoder  $f(\cdot; \theta_f)$  and classifier  $g(\cdot; \theta_g)$  trained on source data  $\mathcal{D}_{train}$ , test-time entropy minimization conducts model learning directly from the testing data  $\mathcal{D}_{test} = \{\mathbf{x}_j\}_{j=1}^M$  by optimizing

$$\min_{\tilde{\theta} \subset \{\theta_f, \theta_g\}} \mathcal{L}(\mathbf{x}; \theta_f, \theta_g) = - \sum_c p(\hat{y}_c) \log p(\hat{y}_c), \quad \text{where } p(\hat{y}_c) = g(f(\mathbf{x}; \theta_f); \theta_g)[c]. \quad (1)$$

Here,  $p(\hat{y}_c)$  denotes the predicted probability for class  $c$ , and  $\tilde{\theta}$  represents the learnable parameters. Based on Eqn. (1), test-time adaptation methods (Wang et al., 2021; Zhang et al., 2022b; Marsden et al., 2024; Zhang et al., 2025) often leverage it to adapt a pretrained model to novel domains under potential distribution shifts, *known as* out-of-distribution generalization. In natural language processing, it has also been employed for large language model alignment and improving predictive performance (Hu et al., 2025a; Jang et al., 2025). By using the model’s own predictive entropy as a self-supervised signal during inference, Eqn. (1) requires neither source data nor modifications to the training process, making it a practical and lightweight solution for real-world deployment.

**Problem Statement and Motivation** As shown in Figure 2 (c-d), model learning with unsupervised entropy minimization on test data may favor non-generalizable shortcuts, such as (i) inflating the logit norm to reduce entropy, or (ii) aligning all logits towards a dominant mode. Such updates converge toward collapsed trivial solutions (*e.g.*, constant one-hot outputs), causing performance degradation. This phenomenon becomes particularly severe in challenging test scenarios or when using weaker base models (*e.g.*, ConvNeXt-Tiny), where the lower source accuracy makes the resulting entropy gradients substantially less reliable, thereby increasing the risk of collapse. Existing methods mainly seek to improve TTA stability with heuristic thresholds to remove some unreliable updates (Niu et al., 2023; Lee et al., 2024), but *the objective is yet trivially minimized by collapsed solutions*. Consequently, prior methods remain exposed to collapse and are sensitive to architectures and domains (see Tables 3-6). This gap motivates us to ask: *How can we design an efficient, theoretically grounded entropy optimization mechanism that inherently avoids undesired trivial solutions?*

## 3 ZEROSIAM: STABLE ADAPTATION VIA MINIMAL ASYMMETRIC NETWORK

We achieve the goal of efficient test-time entropy optimization without collapse by designing a lightweight asymmetric Siamese architecture for entropy minimization, namely ZeroSiam. We draw inspiration from the traditional asymmetric design for similarity learning in SSL, but extend its compatibility to the single-branch entropy minimization via a single learnable predictor—without requiring augmentations and extra backbone passes. We depict the design choice of our ZeroSiam in Section 3.1, and provide further theoretical and empirical evidence of ZeroSiam’s stability for TTA in Section 3.2. The overall details of ZeroSiam are illustrated in Figure 1 (c) and Algorithm 1.

### 3.1 MINIMAL ASYMMETRIC SIAMESE ARCHITECTURE FOR ENTROPY MINIMIZATION

Unlike cross-entropy training supervised by ground-truth labels, test-time entropy minimization relies on the model’s own predicted labels for self-training. This, however, creates a shortcut solution, where the objective can be minimized simply by producing one-hot outputs irrespective of the input. To reach this solution, pure entropy minimization thus tends to inflate the logit norm and drive all predictions toward a dominant class, as illustrated in Figure 2 (c-d), leading to model collapse into degenerate solutions (*e.g.*, constant one-hot outputs). Similar issues appear in negative-free SSL, where the model learns trivial solutions by generating constant representations regardless of inputs

**Algorithm 1** ZeroSiam: Test-Time Asymmetric Entropy Minimization.

---

**Input:** Test samples  $\mathcal{D}_{test} = \{\mathbf{x}_j\}_{j=1}^M$ , encoder  $f(\cdot; \theta_f)$ , classifier  $g(\cdot; \theta_g)$ , inserted predictor  $h(\cdot; \theta_h)$   
**Output:** Predictions  $\{p_j^r\}_{j=1}^M$ .  
 Initialize predictor  $h(\cdot; \theta_h) = \text{Identity}$  ; // warm start for fully test-time learning  
**for**  $\mathbf{x}_j \in \mathcal{D}_{test}$  **do**  
 | Compute encoder feature:  $z = f(\mathbf{x}_j; \theta_f)$  ; // augmentation-free, single-pass  
 | Compute target branch outputs  $u^r = g(z; \theta_g)$ ,  $p^r = \text{softmax}(u^r)$  ; // stop-gradient  
 | Compute online branch outputs  $u^o = g(h(z; \theta_h); \theta_g)$ ,  $p^o = \text{softmax}(u^o)$  ;  
 | Update  $\theta_h$  and normalization params  $\theta \subset \theta_f$  via Eqn. (4).  
**end**

---

to maximize representation similarity. SSL (Chen & He, 2021) prevents such collapse by introducing an asymmetry: with a non-identity predictor  $h$  on one branch, and a stop-gradient operation on the other (see Figure 1). Such asymmetry ensures that degenerate constant outputs incur non-zero alignment loss, preventing the *two branches* from collapsing toward the same constant.

Motivated by this, we hypothesize that an asymmetric mechanism, which remains under-explored in entropy optimization, could also prevent undesired trivial solutions and stabilize self-training. However, constructing asymmetry in test-time entropy optimization remains an open question: (1) Unlike contrastive SSL, entropy-based learning relies on *one prediction branch*, making it non-trivial to introduce a Siamese asymmetric structure; (2) Its objective optimizes entropy rather than similarity, offering no pairwise stop-gradient alignment that enables asymmetry as in SSL; (3) Traditional Siamese designs require extra backbone passes, hindering the efficiency for our test-time learning.

To overcome these challenges, our key idea is to embed asymmetry within a single forward pass. We achieve this by inserting a predictor and the stop-gradient operator before the classifier, which aims to decouple a prediction into two *asymmetric* views from the same feature: an online branch (through the predictor) for optimizing entropy, and a target branch (the original logits) for stop-gradient alignment. In this way, it establishes an efficient asymmetric Siamese for entropy optimization, using no augmentations or extra backbone passes, yet still exploiting asymmetric predictor-target alignment to prevent collapsed constant solutions and stabilize adaptation. Formally, let  $f(\cdot; \theta_f)$  denote the encoder,  $g(\cdot; \theta_g)$  the classifier, and  $h(\cdot; \theta_h)$  a lightweight *linear* predictor. Given a test sample  $\mathbf{x}$ , ZeroSiam computes the encoder feature  $z = f(\mathbf{x}; \theta_f)$  once, then define two asymmetric branches:

$$u^r = g(z; \theta_g), \quad \text{(target branch, stop-gradient)} \quad (2)$$

$$u^o = g(h(z; \theta_h); \theta_g), \quad \text{(online branch).} \quad (3)$$

Let  $p^r = \text{softmax}(u^r)$  and  $p^o = \text{softmax}(u^o)$ . The ZeroSiam objective combines entropy minimization on the online branch with an alignment regularizer to the target branch:

$$\mathcal{L} = H(p^o) + \alpha D(p^o \parallel \text{sg}[p^r]), \quad (4)$$

where  $H(p) = -\sum_c p_c \log p_c$  is the prediction entropy,  $D(\cdot \parallel \cdot)$  is a divergence (e.g.,  $\ell_2$  or KL)<sup>1</sup>, and  $\text{sg}[\cdot]$  denotes stop-gradient. Here,  $\theta_h$  is initialized as an identity to ensure a warm start, which quickly diverges during online learning, as shown in Figure 2 (a), creating the asymmetry necessary to prevent collapsed constant solutions. Interestingly, Table 4 shows that even a *randomly initialized* predictor helps prevent collapse in Tent (Wang et al., 2021), highlighting the value of asymmetry itself, despite still underperforming a learnable predictor. In essence, the predictor-stop-gradient asymmetry inherently rules out collapsed constant solutions as valid minima, thereby avoiding collapse and improving stability during online entropy minimization. Unlike BYOL and SimSiam, which rely on augmentations or extra backbone passes, ZeroSiam shows that asymmetry can also be instantiated within pure online entropy minimization in a minimal and efficient manner.

### 3.2 HOW ZEROSIAM RESISTS COLLAPSE: EMPIRICAL AND THEORETICAL INSIGHTS

Although asymmetric designs (e.g., SimSiam for SSL) are known to prevent collapsed trivial solutions, test-time entropy minimization poses new challenges like logit norm inflation and single-class

<sup>1</sup>ZeroSiam uses symmetric KL loss as  $D(\cdot \parallel \cdot)$  to penalize both under- and over-coverage of modes, i.e.,  $D(p \parallel q) = D_{\text{KL}}(p \parallel q) + D_{\text{KL}}(q \parallel p)$ , and  $\alpha$  is fixed to 1. Results with KL and reverse KL are put in Table 10.

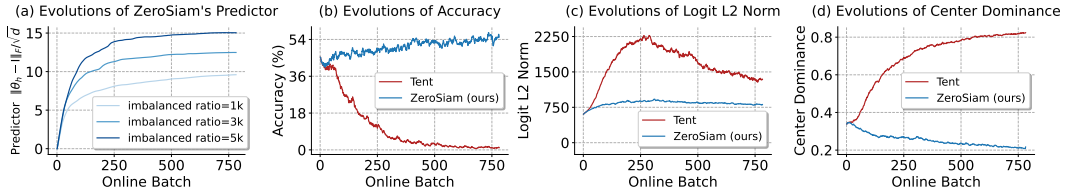


Figure 2: Empirical evidence of ZeroSiam’s stabilization effects. (a) records the Frobenius distance between  $\theta_h$  and the identity matrix under the non-i.i.d. streams with varying imbalance ratios (Niu et al., 2023). (b-d) record the OOD accuracy, logits  $L_2$  norm, and center dominance in model predictions under a mild test scenario (Wang et al., 2021). Center dominance is calculated by  $\|\bar{u}\|/\|u\|$  following (Zhang et al., 2022a). Experiments are conducted on ImageNet-C (Snow, level 5) with ResNet50-GN. For fair comparisons, ZeroSiam and Tent use the same learning rate configuration.

dominance. We find that ZeroSiam not only inherits the anti-collapse effect of asymmetry, *i.e.*, eliminating trivial solutions, but also *plays a broader role* in absorbing bias and regularizing learning dynamics during entropy minimization. In this section, we first present empirical evidence illustrating these stabilizing effects, and further explain ZeroSiam’s behaviors with theoretical insights.

**Empirical Evidence of ZeroSiam’s Stabilization Effects** In Figure 2, we visualize the effects of our ZeroSiam under the unsupervised TTA. We conduct experiments with ResNet50-GN on ImageNet-C, and record the evolution of OOD accuracy, representative failure modes of entropy-based TTA, and changes in predictor parameters  $\theta_h$  (*i.e.*, a single FC layer, learning preliminarily non-generalizable modes due to capacity). From the results, we highlight two key observations:

**Observation 1: Predictor as an Effective Absorber of Biased Learning Signals.** Figure 2 (a) shows that the predictor parameters  $\theta_h$  deviate more rapidly and substantially from the identity mapping when facing online data streams with a higher label imbalance ratio (Niu et al., 2023), which produces more biased signals for entropy minimization that may result in collapse. Here, the large deviation actually acts as a shortcut direction that reduces the target entropy loss to trivial solutions (see also Theorem 1). In this sense, this pronounced deviation thus implies an active absorption of biased learning signals in predictor  $h$ , where such bias is then exposed in the online branch, resulting in a high alignment loss to the target branch, as shown in Figure C in Appendix.

**Observation 2: Asymmetry Suppresses Learning Non-Generalizable Collapse Modes.** In Figure 2 (c), the logit  $L_2$  norm under Tent suffers from a rapid inflation, whereas ZeroSiam grows slowly and then stabilizes. In Figure 2 (d), Tent increasingly aligns logits toward a dominant mode (higher center dominance), while our ZeroSiam suppresses such dominance over time. Consequently, Tent collapses into non-generalizable shortcuts, whereas ZeroSiam mitigates them and achieves better generalization as shown in Figure 2 (b), similarly even when no collapse occurs (see Figure B).

Overall, we observe that the lightweight, linear design of the predictor  $h$  makes it especially sensitive and effective to absorb non-generalizable shortcuts induced by entropy minimization. Meanwhile, the asymmetry in ZeroSiam helps regulate such biases, yielding improved TTA efficacy and stability. This reveals a distinct advantage of ZeroSiam for the unsupervised TTA, and provides TTA-specific evidence on the role of asymmetry in preventing collapse that extends prior self-supervised findings.

**Theoretical Insights of ZeroSiam’s Mechanism** We provide a theoretical analysis to explain ZeroSiam’s behaviors, showing that (i) the predictor enhances the online branch’s dynamism in exploring the parameter space, thereby facilitating more efficient entropy optimization; (ii) the alignment term explicitly regulates the biased learning signals induced by entropy minimization, preventing the model from being exposed to collapsed trivial solutions and meanwhile prompting performance.

**Theorem 1. (Optimization and Stability of ZeroSiam)** Consider the ZeroSiam objective  $\mathcal{L} = H(p^o) + \alpha D(p^o \| \text{sg}[p^r])$ , where  $H(\cdot)$  denotes the entropy loss,  $D(\cdot)$  the alignment regularizer, and  $p^o, p^r \in \Delta^{|\mathcal{C}|-1}$  are the probability distributions induced by the online and target branches. Given the encoder  $f$ , classifier  $g$  and predictor  $h$ . Under Assumptions 1 and 2, the following hold:  
(1) For  $\alpha = 0$ , the entropy variation satisfies  $|\Delta H(p^o)| > |\Delta H(p^r)|$ , and the Hessian of  $H(p^o)$  attains its minimal eigenvalue along collapse directions  $\mathbf{v}$ :

$$\lambda_{\min}(\nabla^2 H(p^o)) = \mathbf{v}^\top \nabla^2 H(p^o) \mathbf{v}.$$

(2) For  $\alpha > 0$ , the predictor  $h$  serves as a filtering mechanism that suppresses gradient update directions corresponding to over-amplified logits, and the system converges to a stable equilibrium: there exists  $h_{\min} > 0$  such that

$$H(p^o) > h_{\min}, p^o \rightarrow p^r.$$

**Remark 1.** Theorem 1 characterizes ZeroSiam’s optimization dynamics and convergence behavior. Initially, the online and target branches coincide within the non-collapse region, so entropy minimization dominates. In this regime, the online branch exhibits a stronger tendency toward collapse than the target branch in both magnitude and directional dominance (Conclusion (1)). As optimization proceeds, the alignment term  $D(\cdot)$  constrains the predictor  $h$  to filter/suppress the gradient components that drive  $p^o$  away from  $p^r$ , i.e., regulating the biased learning signals that may result in collapse, guiding the system toward a stable and non-collapsing equilibrium (Conclusion (2)).

## 4 COMPARISONS WITH STATE-OF-THE-ARTS

**Dataset and Methods** For image classification, we conduct experiments based on ImageNet-C (Hendrycks & Dietterich, 2019), a large-scaled benchmark for out-of-distribution generalization. It contains 15 types of 4 main categories (noise, blur, weather, digital) corrupted images and each type has 5 severity levels. For natural language reasoning, we assess logical reasoning capabilities on Math-500 (Lightman et al., 2023), CollegeMath (Tang et al., 2024), AIME24, and Minerva (Lewkowycz et al., 2022), ranging from high-school mathematics to advanced competition problems. We compare with the following methods. EATA (Niu et al., 2022), SAR (Niu et al., 2023), DeYO (Lee et al., 2024), and CETA (Yang et al., 2024) are entropy-based methods with sample selection or update reweighting. COME (Zhang et al., 2025) predefines an uncertainty mass, implemented based on DeYO for comparisons. TLM (Hu et al., 2025a) refines the prediction entropy on input sequences.

**Models and Implementation Details** We conduct experiments on ResNet50-GN, ViT-Base, ViT-Small, ConvNeXt-Tiny, and Swin-Tiny that are obtained from `timm` (Wightman, 2019) for image classification, and Llama3.1-8B-Instruct (Dubey et al., 2024) for natural language reasoning. We use symmetric KL as the divergence term in Eqn. (4), and  $\alpha$  is fixed to 1 without tuning. We update predictor params  $\theta_h$ , and the affine parameters in norm layers for the vision task per Tent (Wang et al., 2021), and the LoRA (Hu et al., 2022) parameters for LLM. More details are put in Appendix C.

### 4.1 ROBUSTNESS TO CORRUPTION UNDER VARIOUS WILD TEST SETTINGS

In this section, we evaluate the robustness of ZeroSiam under the wild test scenarios as established by SAR (Niu et al., 2023), which simulate practical TTA scenarios in real-world applications, including 1) **online imbalanced label distribution shifts**: the samples in a non-i.i.d. data stream come in class order (in Table 3), 2) **mixed distribution shifts**: the samples in online data stream are obtained from a mixture of 15 corruption types (a total of  $15 \times 50,000$  images) in ImageNet-C, i.e., a prolonged TTA scenario with multiple concurrent shifts (in Table 2), and 3) **batch size = 1**: the samples come one-by-one due to the scarcity of data in online streams (in Table 4). Compared to SAR, we extend the evaluations using more models, including ViT-Small, ConvNeXt-Tiny, and Swin-Tiny.

From the results, we have the following general observations: 1) *Sensitivity on model choice*: While sample selection methods like DeYO perform competitively on ResNet50-GN and ViT-Base, they remain unstable and *sensitive to model choices*, particularly with weaker models where pseudo labels are highly unreliable, e.g., the accuracy of 0.1% (DeYO) vs. 26.5% (ZeroSiam) on *noise* corruptions with ViT-Small under the label shift scenario in Table 3, and SAR and COME also fail to perform TTA (worse than NoAdapt) on Swin-Tiny under mixed shifts in Table 2; 2) *Sensitivity on test scenario choice*: For example, compared to results in Table 3 under label shifts, DeYO’s performance drops

Table 1: Efficiency comparison for processing 50,000 images (Gaussian noise, level 5 on ImageNet-C) via an RTX 3090 GPU on ViT-Base.

Method	GPU time
Tent (Wang et al., 2021)	193 secs
SAR (Niu et al., 2023)	382 secs
EATA (Niu et al., 2022)	197 secs
COME (Zhang et al., 2025)	300 secs
DeYO (Lee et al., 2024)	280 secs
ZeroSiam (ours)	193 secs

Table 2: Comparisons with state-of-the-arts on ImageNet-C (level 5) under **MIXTURE OF 15 CORRUPTION TYPES** w.r.t. **Acc (%)**.

Method	R-50	Vit-B	Vit-S	Con-T	Swi-T	Avg.
NoAdapt	30.6	29.9	22.9	34.7	31.3	29.9
Tent	<b>13.4</b>	<b>16.5</b>	<b>7.1</b>	<b>27.8</b>	<b>6.7</b>	14.3
SAR	38.1	55.7	41.3	36.5	<b>25.9</b>	39.5
EATA	38.3	57.1	36.9	41.1	41.3	42.9
COME	<b>30.0</b>	58.5	40.9	<b>23.7</b>	<b>19.1</b>	34.4
DeYO	38.6	59.4	35.9	<b>27.8</b>	<b>29.0</b>	38.1
ZeroSiam	40.4	57.1	41.7	42.4	39.3	<b>44.2</b>

Table 3: Comparisons with SOTAs on ImageNet-C (level 5) under **ONLINE LABEL SHIFTS** (im-balance ratio= $\infty$ ) w.r.t. **Acc(%)**. “ $\mathcal{N}/\mathcal{B}/\mathcal{W}/\mathcal{D}$ ” are short for *Noise/Blur/Weather/Digital* corruptions. **RED** marks results worse than NoAdapt. **Detailed results of each corruption are put in Appendix.**

Method	ResNet50-GN				ViT-Base				ViT-Small				ConvNeXt-Tiny				Swin-Tiny				Avg.
	$\mathcal{N}$	$\mathcal{B}$	$\mathcal{W}$	$\mathcal{D}$																	
NoAdapt	18.6	19.4	47.7	33.9	8.1	28.4	36.1	41.6	1.8	23.4	27.7	33.5	23.7	24.8	52.1	35.4	25.8	21.7	50.5	25.9	29.0
Tent	<b>2.9</b>	<b>14.6</b>	<b>27.7</b>	38.0	22.9	54.3	41.3	64.7	<b>0.3</b>	40.5	38.5	48.2	<b>22.8</b>	<b>22.9</b>	<b>50.2</b>	<b>34.4</b>	<b>13.6</b>	<b>19.4</b>	<b>34.9</b>	<b>25.3</b>	30.9
SAR	35.0	24.9	47.8	40.6	46.2	55.8	61.4	65.8	<b>1.6</b>	42.2	46.7	52.8	35.5	<b>24.2</b>	<b>43.3</b>	38.0	29.2	<b>19.0</b>	<b>39.4</b>	26.7	38.8
EATA	27.8	20.4	42.7	34.6	35.7	47.4	61.6	51.6	16.3	42.2	54.8	54.2	35.4	29.0	54.9	42.2	35.6	32.9	53.4	41.1	40.7
COME	<b>18.4</b>	<b>19.2</b>	47.7	<b>33.4</b>	49.8	59.2	69.8	67.5	<b>0.2</b>	39.5	56.0	59.6	43.1	<b>24.4</b>	62.9	44.9	42.9	23.9	59.7	27.7	42.5
DeYO	43.7	23.2	54.2	54.5	48.0	56.6	71.2	69.9	<b>0.1</b>	41.4	59.4	60.7	36.0	<b>19.0</b>	<b>43.8</b>	<b>34.8</b>	41.9	26.8	56.6	46.8	44.4
ZeroSiam	43.7	41.2	62.1	57.3	52.8	60.1	71.2	69.6	26.5	50.4	62.0	60.8	43.0	40.0	62.4	53.8	45.3	42.2	59.3	53.6	<b>52.9</b>

Table 4: Comparisons with SOTAs on ImageNet-C (level 5) with **BATCH SIZE=1** w.r.t. **Acc (%)**.

Method	ResNet50-GN				ViT-Base				ViT-Small				ConvNeXt-Tiny				Swin-Tiny				Avg.
	$\mathcal{N}$	$\mathcal{B}$	$\mathcal{W}$	$\mathcal{D}$																	
NoAdapt	18.6	19.4	47.7	33.9	8.1	28.4	36.1	41.7	1.8	23.3	27.8	33.6	23.7	24.6	52.2	35.3	25.9	21.6	50.6	25.8	29.0
Tent	<b>2.6</b>	<b>13.3</b>	<b>27.5</b>	37.9	28.8	51.7	43.7	61.9	23.7	24.6	52.2	35.3	32.0	<b>23.9</b>	<b>51.9</b>	36.5	<b>24.2</b>	23.0	<b>42.1</b>	26.7	33.2
SAR	24.3	23.2	<b>46.9</b>	40.6	39.6	53.7	63.1	64.6	25.9	<b>21.6</b>	50.6	<b>25.8</b>	31.2	25.3	<b>51.0</b>	35.8	<b>25.2</b>	22.8	<b>47.0</b>	26.3	37.2
EATA	26.3	23.3	50.3	43.5	29.8	43.7	52.3	56.4	2.2	30.7	36.9	43.6	28.0	25.1	<b>51.8</b>	36.4	33.0	25.3	<b>50.6</b>	30.8	36.0
COME	<b>18.4</b>	<b>19.3</b>	<b>47.6</b>	<b>33.5</b>	51.7	55.1	70.6	69.6	<b>1.5</b>	41.0	56.7	59.6	41.8	25.5	62.0	43.5	39.7	25.3	58.3	38.6	43.0
DeYO	43.2	28.4	50.2	55.5	53.7	59.0	71.7	70.4	<b>0.5</b>	42.4	59.1	60.4	37.7	<b>21.3</b>	<b>44.2</b>	35.3	36.4	24.6	<b>50.1</b>	35.3	44.0
ZeroSiam	42.6	40.8	62.9	58.6	52.5	59.9	70.9	69.6	27.1	50.1	61.4	60.5	42.2	39.3	61.7	52.8	44.9	41.5	58.8	52.9	<b>52.5</b>

significantly on Swin-Tiny under TTA with a single sample in Table 4, *e.g.*, 46.8% $\rightarrow$ 35.3% regarding the accuracy on *digital* corruptions. This highlights the instability in prior methods and that achieving *robust TTA across diverse architectures and test scenarios remains highly non-trivial*; 3) Our ZeroSiam is simple yet effective. ZeroSiam neither relies on careful sample selection strategies as in SAR or DeYO, nor requires source data as in EATA, and it achieves consistently stable and high performance across models and scenarios, markedly outperforming prior methods, *e.g.*, 52.9% (ZeroSiam) *vs.* 38.8% (SAR) in terms of average accuracy under label shifts in Table 3, and an average gain of +8.5% over DeYO under the batch size of 1 in Table 4, suggesting our effectiveness.

#### 4.2 EFFECTIVENESS FOR INCENTIVIZING REASONING CAPABILITY ONLINE

A statistical reasoning model may fail to generalize to the diverse reasoning tasks in real-world applications, while retraining the model offline is both expensive and time-consuming. We further explore adaptively incentivizing the reasoning capability in a large language model *online*, by minimizing the entropy of its own predicted tokens. From Table 5, we have the following observations: 1) Entropy optimization demonstrates a great potential in enhancing the model’s reasoning online, *i.e.*, all prior methods achieve an accuracy gain by +3.34% on AIME24. 2) However, for a comprehensive benchmark like CollegeMath, covering algebra, calculus, probability, differential equations, *etc*, existing methods may suffer from overfitting and poor generalization, *e.g.*, -0.83% on Tent and -0.75% on SAR. 3) ZeroSiam enhances generalization for online reasoning incentivization with its predictor and asymmetric alignment design, which regularizes non-generalizable shortcuts as discussed in Section 3.2, yielding significant further gains, *e.g.*, +10.00% on AIME24, +3.40% on Math-500, and +3.94% on average. This suggests the potential of our ZeroSiam to boost both the perception robustness and reasoning capability in a model during inference for greater intelligence.

#### 4.3 ROBUSTNESS TO ADVERSARIAL ADAPTATION SCENARIOS (STRESS TEST)

**Robustness under Blind-Spot Adaptation** Existing entropy-based TTA methods largely rely on reliable sample selection strategies to stabilize adaptation (Niu et al., 2023; Lee et al., 2024). However, in many real-world scenarios, adaptation inevitably involves numerous erroneous pseudo labels that cannot be identified, especially when the model’s initial accuracy is very low. This raises a critical concern: How safe is existing TTA in the real world? To stress-test this vulnerability, we construct a *blind-spot subset* consisting only of samples misclassified by the NoAdapt model for each domain and adapt exclusively on this subset, before evaluation on the full dataset. As shown in Table 6, prior methods suffer from severe instability, often collapse and underperform the NoAdapt baseline after TTA, *e.g.*, DeYO deteriorates accuracy on 12 out of 20 scenarios. In contrast, ZeroSiam introduces an efficient asymmetry to prevent undesired trivial solutions from optimization,

Table 5: Comparisons with state-of-the-arts for **ONLINE ADAPTIVE REASONING** in mathematical reasoning benchmarks regarding **Accuracy (%)**.

Model+Method	Math-500	CollegeMath	AIME24	Minerva	Average
Llama3.1-8B (Dubey et al., 2024)	49.20	25.00	3.33	20.96	24.62
• Tent (Wang et al., 2021)	50.00 <sub>(+0.80)</sub>	24.17 <sub>(-0.83)</sub>	6.67 <sub>(+3.34)</sub>	20.59 <sub>(-0.37)</sub>	25.36 <sub>(+0.74)</sub>
• SAR (Niu et al., 2023)	49.20 <sub>(+0.00)</sub>	24.25 <sub>(-0.75)</sub>	6.67 <sub>(+3.34)</sub>	21.32 <sub>(+0.36)</sub>	25.36 <sub>(+0.74)</sub>
• EATA (Niu et al., 2022)	48.80 <sub>(-0.40)</sub>	24.83 <sub>(-0.17)</sub>	6.67 <sub>(+3.34)</sub>	20.59 <sub>(-0.37)</sub>	25.22 <sub>(+0.60)</sub>
• COME (Zhang et al., 2025)	49.80 <sub>(+0.60)</sub>	25.42 <sub>(+0.42)</sub>	6.67 <sub>(+3.34)</sub>	22.74 <sub>(+1.78)</sub>	26.16 <sub>(+1.54)</sub>
• TLM (Hu et al., 2025a)	50.00 <sub>(+0.80)</sub>	25.58 <sub>(+0.58)</sub>	6.67 <sub>(+3.34)</sub>	19.49 <sub>(-1.47)</sub>	25.44 <sub>(+0.82)</sub>
• <b>ZeroSiam (ours)</b>	52.60 <sub>(+3.40)</sub>	26.25 <sub>(+1.25)</sub>	13.33 <sub>(+10.00)</sub>	22.06 <sub>(+1.10)</sub>	<b>28.56</b> <sub>(+3.94)</sub>

Table 6: Comparisons with SOTAs on ImageNet-C (level 5)’s **BLIND-SPOT SUBSET** (samples initially misclassified by the NoAdapt model) with **BATCH SIZE=1** regarding **Accuracy (%)**.

Method	ResNet50-GN				ViT-Base				ViT-Small				ConvNeXt-Tiny				Swin-Tiny				Avg.
	$N$	$B$	$W$	$D$	$N$	$B$	$W$	$D$	$N$	$B$	$W$	$D$	$N$	$B$	$W$	$D$	$N$	$B$	$W$	$D$	
NoAdapt	18.6	19.4	47.7	33.9	8.1	28.4	36.1	41.7	1.8	23.3	27.8	33.6	23.7	24.6	52.2	35.3	25.9	21.6	50.6	25.8	29.0
Tent	<b>0.2</b>	<b>5.2</b>	<b>16.8</b>	<b>28.1</b>	<b>0.2</b>	42.9	<b>20.0</b>	52.0	<b>0.1</b>	40.0	36.3	42.8	<b>17.9</b>	<b>19.7</b>	<b>36.3</b>	<b>31.0</b>	<b>0.2</b>	<b>8.0</b>	<b>22.2</b>	<b>13.0</b>	21.7
SAR	<b>17.9</b>	<b>18.4</b>	<b>35.6</b>	<b>31.6</b>	31.1	55.0	54.0	56.4	2.0	30.4	42.0	43.3	26.4	24.6	<b>50.7</b>	<b>35.1</b>	27.0	22.2	<b>49.3</b>	<b>23.8</b>	33.8
EATA	19.5	<b>19.0</b>	<b>44.2</b>	40.2	26.3	43.5	53.2	57.5	2.0	26.5	32.8	41.7	25.8	24.7	<b>51.6</b>	35.7	27.4	22.4	<b>49.1</b>	26.8	33.5
COME	18.6	19.4	<b>47.6</b>	<b>33.8</b>	<b>0.1</b>	44.8	70.9	69.7	<b>1.0</b>	37.0	55.9	46.2	41.4	<b>16.4</b>	<b>31.1</b>	36.1	40.5	<b>9.5</b>	<b>25.3</b>	26.9	33.6
DeYO	<b>0.5</b>	<b>9.4</b>	<b>21.0</b>	40.0	<b>0.2</b>	47.2	72.6	71.4	<b>0.2</b>	38.2	60.2	61.7	35.2	<b>12.2</b>	<b>35.0</b>	<b>33.0</b>	<b>0.2</b>	<b>8.8</b>	<b>25.7</b>	<b>23.9</b>	29.8
<b>ZeroSiam</b>	39.9	36.6	53.9	52.7	53.0	60.4	71.6	70.2	26.1	49.8	61.8	61.1	43.3	40.3	61.9	55.0	46.5	42.1	58.8	54.7	<b>52.0</b>

delivering consistent accuracy gains *even when adapting with incorrect labels e.g.,* the average accuracy of 29.0% (NoAdapt) vs. 52.0% (ZeroSiam), drastically breaking prior performance ceiling ( $\approx 33.6\%$ ). This underscores ZeroSiam as a more principled and robust solution for real-world TTA.

**Resistance to Learning from Noise** In dynamic real-world applications, models may frequently encounter test data that are severely corrupted and *non-semantic*, such as extreme occluded frames and pure sensor noise where no valid label exists. Minimizing entropy on these data can then be misled to “confidently learn nonsense”, risking model degeneration. To simulate this, we first pre-adapt models on varying amounts of pure Gaussian noise, then perform TTA on ImageNet-C (Fog, level 5) with ViT-Base under the mid scenario (Wang et al., 2021). As shown in Figure 3, existing entropy-based methods degrade sharply post-adaptation to noise, *e.g.*, 67.3% $\rightarrow$ 27.2% on CETA, indicating an overfit to non-semantic patterns. In contrast, ZeroSiam absorbs and regularizes non-generalizable shortcuts through the asymmetric alignment (c.f. Section 3.2), maintaining consistently high and stable accuracy ( $\approx 72\%$ ) regardless of the exposure to noisy inputs. This robustness implies that ZeroSiam can be safely deployed even when streams contain meaningless or corrupted inputs, a property crucial for reliable deployment in real-world scenarios.

#### 4.4 ADDITIONAL DISCUSSIONS

**Efficacy under Mild Test Setting** We further evaluate ZeroSiam in the mild setting (Wang et al., 2021), where data comes with shuffled labels. As shown in Table 7, ZeroSiam delivers superior performance compared to prior method, *e.g.*, the average accuracy of 50.1% (ZeroSiam) vs. 43.0% (COME), suggesting our efficacy across a wide range of scenarios. Moreover, as in Table 1, ZeroSiam also achieves a lower latency compared to prior state-of-the-arts, *e.g.*, 193s (ZeroSiam) vs. 280s (DeYO), highlighting the advantages of ZeroSiam regarding both TTA stability and efficiency.

**Ablation on Predictor Design** We further examine other predictor designs in Table 8. Interestingly, replacing the learnable predictor with a fixed, randomly initialized predictor ( $\theta_h = \mathbf{I} + 0.1 \mathbf{W}$ ,  $\mathbf{W} \sim \mathcal{N}(0, \mathbf{I})$ ) already improves upon Tent, *i.e.*, 47.3% $\rightarrow$ 60.7% w.r.t. accuracy, confirming the value of breaking symmetry alone in collapse mitigation. However, making the predictor deeper and nonlinear brings no further gain (64.0% vs. 64.1%), since the predictor in ZeroSiam is to absorb biased shortcuts for regularization rather than learning rich representations, which do not need large representation capacity. Therefore, we use the single linear predictor for all other experiments.

**Integration with Prior Methods** We further evaluate the efficacy of our ZeroSiam when integrated with state-of-the-art methods. From Table 9, ZeroSiam consistently enhances the performance of

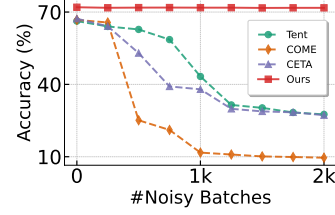


Figure 3: Resistance to learning from noise. Models pre-adapt on  $N$  pure Gaussian noise, then run TTA on ImageNet-C (level 5).

Table 7: Comparisons with state-of-the-art methods on ImageNet-C (severity level 5) under a **MILD SCENARIO** regarding **Accuracy (%)**. “*N/B/W/D*” denote *Noise/Blur/Weather/Digital* corruptions.

Method	ResNet50-GN				ViT-Base				ViT-Small				ConvNeXt-Tiny				Swin-Tiny				Avg.
	<i>N</i>	<i>B</i>	<i>W</i>	<i>D</i>	<i>N</i>	<i>B</i>	<i>W</i>	<i>D</i>	<i>N</i>	<i>B</i>	<i>W</i>	<i>D</i>	<i>N</i>	<i>B</i>	<i>W</i>	<i>D</i>	<i>N</i>	<i>B</i>	<i>W</i>	<i>D</i>	
NoAdapt	18.6	19.4	47.7	33.9	8.1	28.4	36.1	41.6	1.8	23.4	27.7	33.5	23.7	24.8	52.1	35.4	25.8	21.7	50.5	25.9	29.0
Tent	<b>5.5</b>	<b>17.7</b>	<b>33.1</b>	39.0	29.0	51.3	44.7	62.1	<b>0.5</b>	37.2	41.4	47.2	32.1	<b>24.0</b>	<b>51.9</b>	36.6	<b>24.2</b>	23.1	<b>42.6</b>	26.9	33.5
SAR	29.9	24.6	<b>41.2</b>	41.8	34.7	52.4	62.5	62.6	<b>1.5</b>	38.6	44.1	49.0	34.2	25.0	<b>45.4</b>	37.8	32.4	25.1	<b>47.3</b>	29.0	38.0
EATA	38.6	32.8	56.9	51.4	50.1	57.4	68.2	67.2	22.2	44.7	56.4	56.2	36.2	30.6	55.5	42.6	41.8	37.5	56.5	47.1	47.5
COME	<b>18.4</b>	<b>19.3</b>	<b>47.6</b>	<b>33.6</b>	51.6	58.9	70.1	69.0	<b>0.3</b>	41.2	56.0	58.4	41.1	26.3	60.5	43.4	42.2	25.5	58.7	38.6	43.0
DEYO	40.8	30.4	<b>44.0</b>	51.4	53.3	55.0	71.1	69.6	<b>0.2</b>	44.7	57.8	59.0	37.3	<b>22.1</b>	<b>44.3</b>	36.2	36.1	24.6	51.0	41.1	43.5
<i>ZeroSiam</i>	41.6	37.1	59.7	54.2	51.0	58.4	69.6	68.3	24.2	48.1	59.6	58.8	40.2	35.4	59.5	49.0	43.1	38.2	56.6	49.8	<b>50.1</b>

Table 8: Ablation on predictor design in ZeroSiam on ImageNet-C (level 5) with ViT-Base under label shifts.

Method	Predictor	Acc.
Tent	-	47.3
ZeroSiam	FC	<b>64.1</b>
• Exp1	<i>fixed</i> random FC	60.7
• Exp2	FC+ReLU+FC	64.0

Table 9: ZeroSiam’s efficacy when used with prior methods. Experiments are on ImageNet-C (level 5) under label shifts.

Method	ViT-B	R-50	Con-T	Avg.
EATA	49.4	31.6	40.7	40.6
+ ZeroSiam	57.1	48.3	41.7	49.0
DeYO	62.3	43.9	33.2	46.5
+ ZeroSiam	65.0	50.7	46.1	53.9

Table 10: Generality of ZeroSiam across objective and divergence choices on ImageNet-C (level 5) with ViT-Base under label shifts.

Loss	N/A	sKL	KL	rKL	JS	MSE
SLR	44.0	62.2	63.2	61.0	63.4	61.5
CE	43.2	61.6	61.4	61.9	61.4	62.1
-p <sup>2</sup>	45.8	63.3	63.4	62.1	63.0	63.6
Tent	47.3	64.1	64.0	64.1	63.8	64.1

prior methods, *e.g.*, improving the average accuracy by +8.4% on EATA and +7.4% on DeYO, suggesting the efficacy of our asymmetric architecture as a plug-and-play component. However, incorporating with EATA and DeYO does not ensure an improvement over ZeroSiam. This is because while EATA and DeYO aim to filter partial noisy samples, ZeroSiam adapts reliably even with incorrect pseudo labels, as verified in Table 6. Thus, ZeroSiam may not directly benefit from the traditional sample selection design and encourages more exploration. We leave it for future work.

**Sensitivity to Learning Rates** We further examine the sensitivity of ZeroSiam to learning rates. When the predictor learning rate is set to zero, the predictor becomes a frozen identity and ZeroSiam degenerates to Tent. From Figure 4, we have the following observations: 1) our ZeroSiam consistently outperforms Tent across a wide range of encoder learning rates, *i.e.*, by 11.3%–28.2% in accuracy, suggesting the benefit of our asymmetric design. 2) For a fixed encoder learning rate, varying  $\eta_h \in \{1, 2.5, 5, 7.5, 10\} \times 0.001$  changes accuracy by only  $\approx 1\%$ , highlighting our effectiveness does not rely on careful hyperparameter tuning. 3) overall, ZeroSiam achieves both high accuracy and a broad performance plateau under diverse learning rate configurations, *e.g.*, above 62.3% when  $\eta_f \in [2.5, 10] \times 10^{-3}$  and  $\eta_h \in [1, 10] \times 10^{-3}$ , consistently outperforming the accuracy of 58.0% in SAR. These results suggest that ZeroSiam is not only effective but also robust to learning rate choices, making it practical and easy to use for online deployment.

**Generality of ZeroSiam’s architecture** ZeroSiam introduces a general asymmetric architecture without limiting the use of self-training objectives and divergence terms. As shown in Table 10, ZeroSiam remains effective across a wide range of combinations and consistently outperforms the single-branch baselines, *e.g.*, 44.0% (SLR) vs. 63.2% (SLR+KL). This arises because collapsed solutions and non-generalizable shortcuts remain pervasive across many unsupervised objectives, suggesting a promising direction for extending ZeroSiam to a wider range of tasks in the future. For test-time entropy minimization, we prefer symmetric KL as the divergence, which offers an elegant overall formulation of Eqn. (4) with  $H(p_o, \text{sg}[p_r]) + H(\text{sg}[p_r], p_o)$  by setting  $\alpha=1$  without tuning.

## 5 CONCLUSION

In this paper, we aim to design a new efficient test-time entropy minimization mechanism that can inherently avoid collapsed trivial solutions, improving stability across challenging real-world scenarios. To this end, we devise a lightweight Siamese architecture for asymmetric entropy minimization

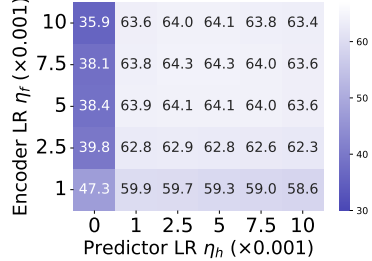


Figure 4: Sensitivity to learning rates. Results are reported on ImageNet-C (level 5) with ViT-Base under label shifts w.r.t. Accuracy.

(termed ZeroSiam) to prevent the model from being exposed to collapsed solutions, using an injected learnable predictor. The predictor converts collapsed solutions into explicit discrepancies, which are then eliminated by an alignment term. We empirically and theoretically demonstrate that ZeroSiam not only prevents collapse but also absorbs and regularizes biased learning signals during learning, thereby boosting the performance even when collapse does not occur. Extensive experiments verify that ZeroSiam performs more stably over prior methods with negligible overhead, proving effective in both vision adaptation and LLM reasoning tasks across challenging models and test scenarios.

## REFERENCES

Zafarali Ahmed, Nicolas Le Roux, Mohammad Norouzi, and Dale Schuurmans. Understanding the impact of entropy on policy optimization. In *International conference on machine learning*, pp. 151–160. PMLR, 2019.

Adrien Bardes, Jean Ponce, and Yann LeCun. Vicreg: Variance-invariance-covariance regularization for self-supervised learning. In *International Conference on Learning Representations*, 2022.

Alexander Bartler, Andre Bühler, Felix Wiewel, Mario Döbler, and Bin Yang. Mt3: Meta test-time training for self-supervised test-time adaption. In *International Conference on Artificial Intelligence and Statistics*, pp. 3080–3090. PMLR, 2022.

Guohao Chen, Shuaicheng Niu, Deyu Chen, Shuhai Zhang, Changsheng Li, Yuanqing Li, and Mingkui Tan. Cross-device collaborative test-time adaptation. In *Advances in Neural Information Processing Systems*, volume 37, pp. 122917–122951, 2024.

Ting Chen, Simon Kornblith, Mohammad Norouzi, and Geoffrey Hinton. A simple framework for contrastive learning of visual representations. In *International Conference on Machine Learning*, pp. 1597–1607, 2020.

Xinlei Chen and Kaiming He. Exploring simple siamese representation learning. In *IEEE Conference on Computer Vision and Pattern Recognition*, pp. 15750–15758, 2021.

MAA Codeforces. American invitational mathematics examination-aime, 2024.

Jia Deng, Wei Dong, Richard Socher, Li-Jia Li, Kai Li, and Li Fei-Fei. Imagenet: A large-scale hierarchical image database. In *IEEE Conference on Computer Vision and Pattern Recognition*, pp. 248–255, 2009.

Zeshuai Deng, Guohao Chen, Shuaicheng Niu, Hui Luo, Shuhai Zhang, Yifan Yang, Renjie Chen, Wei Luo, and Mingkui Tan. Test-time model adaptation for quantized neural networks. *arXiv preprint arXiv:2508.02180*, 2025.

Abhimanyu Dubey, Abhinav Jauhri, Abhinav Pandey, Abhishek Kadian, Ahmad Al-Dahle, Aiesha Letman, Akhil Mathur, Alan Schelten, Amy Yang, Angela Fan, et al. The llama 3 herd of models. *arXiv e-prints*, pp. arXiv–2407, 2024.

Yossi Gandelsman, Yu Sun, Xinlei Chen, and Alexei Efros. Test-time training with masked autoencoders. In *Advances in Neural Information Processing Systems*, volume 35, pp. 29374–29385, 2022.

Yves Grandvalet and Yoshua Bengio. Semi-supervised learning by entropy minimization. In *Advances in Neural Information Processing Systems*, volume 17, 2004.

Jean-Bastien Grill, Florian Strub, Florent Altché, Corentin Tallec, Pierre Richemond, Elena Buchatskaya, Carl Doersch, Bernardo Avila Pires, Zhaohan Guo, Mohammad Gheshlaghi Azar, et al. Bootstrap your own latent-a new approach to self-supervised learning. In *Advances in neural information processing systems*, volume 33, pp. 21271–21284, 2020.

Tuomas Haarnoja, Aurick Zhou, Pieter Abbeel, and Sergey Levine. Soft actor-critic: Off-policy maximum entropy deep reinforcement learning with a stochastic actor. In *International Conference on Machine Learning*, pp. 1861–1870. Pmlr, 2018.

Kaiming He, Haoqi Fan, Yuxin Wu, Saining Xie, and Ross Girshick. Momentum contrast for unsupervised visual representation learning. In *Proceedings of the IEEE/CVF conference on computer vision and pattern recognition*, pp. 9729–9738, 2020.

Dan Hendrycks and Thomas Dietterich. Benchmarking neural network robustness to common corruptions and perturbations. In *International Conference on Learning Representations*, pp. 1–11, 2019.

Dan Hendrycks, Collin Burns, Saurav Kadavath, Akul Arora, Steven Basart, Eric Tang, Dawn Song, and Jacob Steinhardt. Measuring mathematical problem solving with the math dataset. In *Thirty-fifth Conference on Neural Information Processing Systems Datasets and Benchmarks Track (Round 2)*, 2021.

Edward J Hu, Phillip Wallis, Zeyuan Allen-Zhu, Yuanzhi Li, Shean Wang, Lu Wang, Weizhu Chen, et al. Lora: Low-rank adaptation of large language models. In *International Conference on Learning Representations*, 2022.

Jinwu Hu, Zitian Zhang, Guohao Chen, Xutao Wen, Chao Shuai, Wei Luo, Bin Xiao, Yuanqing Li, and Mingkui Tan. Test-time learning for large language models. In *International Conference on Machine Learning*. PMLR, 2025a.

Zixuan Hu, Yichun Hu, Xiaotong Li, Shixiang Tang, and Lingyu Duan. Beyond entropy: Region confidence proxy for wild test-time adaptation. In *International Conference on Machine Learning*, 2025b.

Hyosoon Jang, Yunhui Jang, Sungjae Lee, Jungseul Ok, and Sungsoo Ahn. Self-training large language models with confident reasoning. *arXiv preprint arXiv:2505.17454*, 2025.

Jing Jiang and ChengXiang Zhai. Instance weighting for domain adaptation in nlp. In *Annual Meeting of the Association for Computational Linguistics*, 2007.

Chi Jin, Rong Ge, Praneeth Netrapalli, Sham M Kakade, and Michael I Jordan. How to escape saddle points efficiently. In *International conference on machine learning*, pp. 1724–1732. PMLR, 2017.

Dong-Hyun Lee et al. Pseudo-label: The simple and efficient semi-supervised learning method for deep neural networks. In *Workshop on challenges in representation learning, ICML*, 2013.

Jonghyun Lee, Dahuin Jung, Saehyung Lee, Junsung Park, Juhyeon Shin, Uiwon Hwang, and Sung-roh Yoon. Entropy is not enough for test-time adaptation: From the perspective of disentangled factors. In *International Conference on Learning Representations*, 2024.

Aitor Lewkowycz, Anders Andreassen, David Dohan, Ethan Dyer, Henryk Michalewski, Vinay Ramasesh, Ambrose Slone, Cem Anil, Imanol Schlag, Theo Gutman-Solo, et al. Solving quantitative reasoning problems with language models. In *Advances in Neural Information Processing Systems*, volume 35, pp. 3843–3857, 2022.

Jian Liang, Ran He, and Tieniu Tan. A comprehensive survey on test-time adaptation under distribution shifts. *International Journal of Computer Vision*, 133(1):31–64, 2025.

Hunter Lightman, Vineet Kosaraju, Yuri Burda, Harrison Edwards, Bowen Baker, Teddy Lee, Jan Leike, John Schulman, Ilya Sutskever, and Karl Cobbe. Let’s verify step by step. In *The Twelfth International Conference on Learning Representations*, 2023.

Yuejiang Liu, Parth Kothari, Bastien van Delft, Baptiste Bellot-Gurlet, Taylor Mordan, and Alexandre Alahi. Ttt++: When does self-supervised test-time training fail or thrive? In *Advances in Neural Information Processing Systems*, volume 34, pp. 21808–21820, 2021.

Mingsheng Long, Han Zhu, Jianmin Wang, and Michael I Jordan. Unsupervised domain adaptation with residual transfer networks. In *Advances in Neural Information Processing Systems*, volume 29, 2016.

Robert A Marsden, Mario Döbler, and Bin Yang. Universal test-time adaptation through weight ensembling, diversity weighting, and prior correction. In *Winter Conference on Applications of Computer Vision*, pp. 2555–2565, 2024.

Volodymyr Mnih, Koray Kavukcuoglu, David Silver, Andrei A Rusu, Joel Veness, Marc G Bellemare, Alex Graves, Martin Riedmiller, Andreas K Fidjeland, Georg Ostrovski, et al. Human-level control through deep reinforcement learning. *nature*, 518(7540):529–533, 2015.

Volodymyr Mnih, Adria Puigdomenech Badia, Mehdi Mirza, Alex Graves, Timothy Lillicrap, Tim Harley, David Silver, and Koray Kavukcuoglu. Asynchronous methods for deep reinforcement learning. In *International conference on machine learning*, pp. 1928–1937. PMLR, 2016.

Pietro Morerio, Jacopo Cavazza, and Vittorio Murino. Minimal-entropy correlation alignment for unsupervised deep domain adaptation. *arXiv preprint arXiv:1711.10288*, 2017.

Michał Nauman, Mateusz Ostaszewski, Krzysztof Jankowski, Piotr Miłoś, and Marek Cygan. Bigger, regularized, optimistic: scaling for compute and sample efficient continuous control. *Advances in neural information processing systems*, 37:113038–113071, 2024.

Shuaicheng Niu, Jiaxiang Wu, Yifan Zhang, Yaofo Chen, Shijian Zheng, Peilin Zhao, and Mingkui Tan. Efficient test-time model adaptation without forgetting. In *International Conference on Machine Learning*, pp. 16888–16905. PMLR, 2022.

Shuaicheng Niu, Jiaxiang Wu, Yifan Zhang, Zhiqian Wen, Yaofo Chen, Peilin Zhao, and Mingkui Tan. Towards stable test-time adaptation in dynamic wild world. In *International Conference on Learning Representations*, pp. 1–14, 2023.

Shuaicheng Niu, Chunyan Miao, Guohao Chen, Pengcheng Wu, and Peilin Zhao. Test-time model adaptation with only forward passes. In *International Conference on Machine Learning*, 2024.

Shuaicheng Niu, Guohao Chen, Deyu Chen, Yifan Zhang, Jiaxiang Wu, Zhiqian Wen, Yaofo Chen, Peilin Zhao, Chunyan Miao, and Mingkui Tan. Adapt in the wild: Test-time entropy minimization with sharpness and feature regularization. *arXiv preprint arXiv:2509.04977*, 2025a.

Shuaicheng Niu, Guohao Chen, Peilin Zhao, Tianyi Wang, Pengcheng Wu, and Zhiqi Shen. Self-bootstrapping for versatile test-time adaptation. In *International Conference on Machine Learning*, 2025b.

Aaron van den Oord, Yazhe Li, and Oriol Vinyals. Representation learning with contrastive predictive coding. *arXiv preprint arXiv:1807.03748*, 2018.

Mehdi Sajjadi, Mehran Javanmardi, and Tolga Tasdizen. Regularization with stochastic transformations and perturbations for deep semi-supervised learning. In *Advances in Neural Information Processing Systems*, volume 29, 2016.

Nikunj Saunshi, Orestis Plevrakis, Sanjeev Arora, Mikhail Khodak, and Hrishikesh Khandeparkar. A theoretical analysis of contrastive unsupervised representation learning. In *International conference on machine learning*, pp. 5628–5637. PMLR, 2019.

John Schulman, Sergey Levine, Pieter Abbeel, Michael Jordan, and Philipp Moritz. Trust region policy optimization. In *International conference on machine learning*, pp. 1889–1897. PMLR, 2015.

John Schulman, Filip Wolski, Prafulla Dhariwal, Alec Radford, and Oleg Klimov. Proximal policy optimization algorithms. *arXiv preprint arXiv:1707.06347*, 2017.

Max Schwarzer, Johan Samir Obando Ceron, Aaron Courville, Marc G Bellemare, Rishabh Agarwal, and Pablo Samuel Castro. Bigger, better, faster: Human-level atari with human-level efficiency. In *International Conference on Machine Learning*, pp. 30365–30380. PMLR, 2023.

Yu Sun, Xiaolong Wang, Zhuang Liu, John Miller, Alexei Efros, and Moritz Hardt. Test-time training with self-supervision for generalization under distribution shifts. In *International Conference on Machine Learning*, pp. 9229–9248, 2020.

Mingkui Tan, Guohao Chen, Jiaxiang Wu, Yifan Zhang, Yaofo Chen, Peilin Zhao, and Shuaicheng Niu. Uncertainty-calibrated test-time model adaptation without forgetting. *IEEE Transactions on Pattern Analysis and Machine Intelligence*, 2025.

Zhengyang Tang, Xingxing Zhang, Benyou Wang, and Furu Wei. Mathscale: Scaling instruction tuning for mathematical reasoning. In *Forty-first International Conference on Machine Learning*, 2024.

Dequan Wang, Evan Shelhamer, Shaoteng Liu, Bruno Olshausen, and Trevor Darrell. Tent: Fully test-time adaptation by entropy minimization. In *International Conference on Learning Representations*, pp. 1–12, 2021.

Ross Wightman. Pytorch image models. <https://github.com/rwightman/pytorch-image-models>, 2019.

Shoukai Xu, Mingkui Tan, Liu Liu, Zhong Zhang, Peilin Zhao, et al. Test-time adapted reinforcement learning with action entropy regularization. In *International Conference on Machine Learning*, 2025.

Hao Yang, Min Wang, Jinshen Jiang, and Yun Zhou. Towards test time adaptation via calibrated entropy minimization. In *Proceedings of the 30th ACM SIGKDD Conference on Knowledge Discovery and Data Mining*, pp. 3736–3746, 2024.

Jure Zbontar, Li Jing, Ishan Misra, Yann LeCun, and Stéphane Deny. Barlow twins: Self-supervised learning via redundancy reduction. In *International conference on machine learning*, pp. 12310–12320. PMLR, 2021.

Chaoning Zhang, Kang Zhang, Chenshuang Zhang, Trung X Pham, Chang D Yoo, and In So Kweon. How does simsiam avoid collapse without negative samples? a unified understanding with self-supervised contrastive learning. In *International Conference on Learning Representations*, 2022a.

Marvin Mengxin Zhang, Sergey Levine, and Chelsea Finn. Memo: Test time robustness via adaptation and augmentation. In *Advances in Neural Information Processing Systems*, pp. 38629–38642, 2022b.

Qingyang Zhang, Yatao Bian, Xinkai Kong, Peilin Zhao, and Changqing Zhang. Come: Test-time adaption by conservatively minimizing entropy. In *International Conference on Learning Representations*, 2025.

Brian D Ziebart, Andrew L Maas, J Andrew Bagnell, Anind K Dey, et al. Maximum entropy inverse reinforcement learning. In *AAAI Conference on Artificial Intelligence*, volume 8, pp. 1433–1438. Chicago, IL, USA, 2008.

Yuxin Zuo, Kaiyan Zhang, Li Sheng, Shang Qu, Ganqu Cui, Xuekai Zhu, Haozhan Li, Yuchen Zhang, Xinwei Long, Ermo Hua, et al. Ttrl: Test-time reinforcement learning. *arXiv preprint arXiv:2504.16084*, 2025.

# APPENDIX

## CONTENTS

<b>A Related Work</b>	<b>15</b>
<b>B Theoretical Analysis</b>	<b>16</b>
B.1 Assumptions . . . . .	16
B.2 Proof of Lemma 1 . . . . .	16
B.3 Proof of Lemma 2 . . . . .	17
B.4 Proof of Theorem 1 . . . . .	18
<b>C More Implementation Details</b>	<b>21</b>
C.1 More Details on Dataset . . . . .	21
C.2 More Experimental Protocols . . . . .	21
<b>D More experimental results</b>	<b>24</b>
D.1 Detailed and Additional Results under Wild Test Scenarios . . . . .	24
D.2 Detailed Results for TTA on the Blind-Spot Subset . . . . .	24
D.3 Detailed Results under the Mild Test Scenario . . . . .	24
<b>E Additional Discussions</b>	<b>27</b>
E.1 ZeroSiam’s Efficacy beyond Collapse Prevention . . . . .	27
E.2 Evolutions of Divergence Loss in ZeroSiam . . . . .	27
E.3 ZeroSiam for Saving a Collapsed Model . . . . .	28
E.4 Sensitivity of $\alpha$ in ZeroSiam . . . . .	28
E.5 Necessity of Stop-gradient for Asymmetry . . . . .	28
<b>F More Discussions with Reinforcement Learning</b>	<b>29</b>

## A RELATED WORK

In this section, we connect test-time entropy minimization and self-supervised learning through their shared challenge of collapse, and relate our approach to these areas.

**Test-Time Entropy minimization** seeks to promote confident predictions by minimizing the prediction entropy on test data. Tent (Wang et al., 2021) first exploits this scheme for test-time model adaptation to novel and out-of-distribution environments. Unlike *test-time training* approaches (Sun et al., 2020; Liu et al., 2021; Bartler et al., 2022; Gandelsman et al., 2022), which train an extra auxiliary self-supervised branch to produce learning signals from test data, test-time entropy minimization (Wang et al., 2021; Niu et al., 2022; Marsden et al., 2024; Lee et al., 2024; Zhang et al., 2025; Hu et al., 2025b; Niu et al., 2025a) removes reliance on the source training process and adapts an arbitrary model on-the-fly by using its own predicted labels for self-training, establishing the fully test-time adaptation paradigm that is more practical in real-world applications (Niu et al., 2024; Tan et al., 2025; Deng et al., 2025; Liang et al., 2025; Niu et al., 2025b). Test-time entropy optimization has attracted growing interest in various fields, such as incentivizing knowledge in large language models during inference (Jang et al., 2025; Zuo et al., 2025; Hu et al., 2025a), and adapting a fixed policy network to evolving environments in real-time (Xu et al., 2025), showing great potential.

Nevertheless, as highlighted by Niu et al. (2023), entropy minimization is inherently unstable and prone to collapse, *e.g.*, converging towards constant one-hot outputs that trivially minimize the entropy loss without meaningful predictions. To improve stability, subsequent methods explored strategies such as sample filtering (Niu et al., 2023; Lee et al., 2024; Hu et al., 2025a), uncertainty quantification (Zhang et al., 2025), and parameter restoration (Chen et al., 2024; Marsden et al., 2024). Despite these advances, collapsed constant solutions remain valid optima in prior methods, so stability often hinges on heuristics, thresholds, or extra compute, leaving methods sensitive to architectures and domains, where robust architectural design is largely underexplored. Our ZeroSiam fills this gap by introducing asymmetry that rules out trivial minima in test-time entropy minimization, while remaining efficient by avoiding augmentations and extra encoder passes.

**Self-supervised Learning** aims to learn discriminative and consistent representations by creating pretext tasks such as contrastive learning (Oord et al., 2018; Saunshi et al., 2019; He et al., 2020; Chen et al., 2020). A central challenge in SSL is trivial collapse, where all outputs degenerate to a constant to maximize representation similarity. Contrastive methods such as SimCLR (Chen et al., 2020) and MoCo (He et al., 2020) prevent collapse by pushing apart negative pairs, but rely on large batch sizes, memory banks, or careful negative mining strategies. To remove dependency on negative samples, BYOL (Grill et al., 2020) and SimSiam (Chen & He, 2021) introduce asymmetric architectures, preventing collapse with a *predictor-stop-gradient asymmetry* to break the stability of the collapsed constant solution. Although subsequent methods such as Barlow Twins (Zbontar et al., 2021) and VicReg (Bardes et al., 2022) achieve stability without symmetry-breaking design by maximizing feature diversity within a batch, they implicitly assume large batches and i.i.d. streams, which often fail during testing. Inspired by SimSiam, we revisit asymmetry in the context of single-branch, entropy-based TTA, and show how it can be instantiated in a minimal and efficient manner.

## B THEORETICAL ANALYSIS

**Notations.** Let  $\mathcal{L} = H(p^o) + \alpha D(p^o \parallel \text{sg}[p^r])$  be the optimization objective of ZeroSiam, where  $H(\cdot)$  is the entropy loss,  $D(\cdot)$  the alignment regularizer, and  $p^o, p^r \in \Delta^{|\mathcal{C}|-1}$  are the probability distributions induced by the online and target branches. Let the encoder  $f$  and classifier  $g$  be pretrained, and  $h$  a lightweight *linear* predictor. At initialization, we set  $h$  as the identity mapping  $\mathbf{I}$ , so that the online and target branches coincide and both lie in the non-collapse region  $\{p \in \Delta^{|\mathcal{C}|-1} \mid \min_c p_c \geq \delta > 0\}$ .

### B.1 ASSUMPTIONS

**Assumption 1. (Lipschitz continuity of the encoder)** Let  $f(\cdot; \theta_f)$  be an encoder parameterized by  $\theta_f$ . We assume  $f$  is Lipschitz continuous with respect to its parameters. Specifically, there exists a constant  $L_f > 0$  such that for any  $\theta_1, \theta_2$  and any input  $\mathbf{x}$  in the domain,

$$\|f_{\theta_1}(\mathbf{x}) - f_{\theta_2}(\mathbf{x})\|_2 \leq L_f \|\theta_1 - \theta_2\|.$$

Assumption 1 bounds the sensitivity of the encoder  $f$  to parameter perturbations, thereby ensuring stability for subsequent optimization analysis. Given that only the affine parameters of the normalization layers are optimized, this assumption is well justified.

**Assumption 2. (Standard optimization assumptions)** Let  $\mathcal{L}(\cdot)$  denote the objective function,  $\phi = (\theta_h, \theta_f)$  the set of optimization parameters, and  $\eta_h, \eta_f$  the learning rates for the predictor and encoder, respectively. Our analysis relies on the following standard assumptions, which are common in the optimization literature:

(1) *Smoothness:*  $\mathcal{L}$  is  $\rho$ -smooth. Specifically, there exists  $\rho > 0$  such that for all  $\phi_1, \phi_2$ ,

$$\|\nabla_\phi \mathcal{L}(\phi_1) - \nabla_\phi \mathcal{L}(\phi_2)\| \leq \rho \|\phi_1 - \phi_2\|;$$

(2) *Descent condition:* The learning rates satisfy  $\max(\eta_h, \eta_f) < \frac{1}{\rho}$ , ensuring monotonic descent.

Assumption 2 constrains the appropriate range of learning rates to guarantee monotonic descent of  $\mathcal{L}(\cdot)$ , which is a common assumption in optimization research.

### B.2 PROOF OF LEMMA 1

**Lemma 1. (Gradient dominance in entropy descent)** Let  $H(\cdot)$  denote the entropy function,  $g(\cdot; \theta_g), h(\cdot; \theta_h)$  and  $f(\cdot; \theta_f)$  denote the classifier, the predictor and the encoder,  $\phi = (\theta_h, \theta_f)$  the set of optimization parameters, and  $\eta_h, \eta_f$  the learning rates for the predictor and encoder, respectively. Then the discrete change in entropy of the target branch satisfies:

$$\|\nabla_\phi H(p^o(t))\| \geq \frac{1}{L_H \|g\|_2 L_f \cdot \max(\eta_h, \eta_f)} \cdot |H(p^r(t+1)) - H(p^r(t))|,$$

where  $L_H, L_f$  are the Lipschitz constants of  $H(\cdot)$  and  $f$ ,  $\|g\|_2$  denotes the spectral norm of the classifier weight vector, and  $t$  is the optimization iteration step.

*Proof.* Consider the online and target branches:

$$\begin{cases} p^o = \text{softmax}(g(h(f(\mathbf{x}; \theta_f); \theta_h); \theta_g)) & \text{(online branch),} \\ p^r = \text{softmax}(g(f(\mathbf{x}; \theta_f); \theta_g)) & \text{(target branch).} \end{cases}$$

By design, the encoder  $f$  of the target branch is synchronized with the online branch after each update:

$$\theta_f^r(t+1) = \theta_f^o(t+1) = \theta_f^o(t) - \eta_f \nabla_{\theta_f} H(p^o(t)).$$

Thus, we bound the entropy change of the target branch  $|H(p^r(t+1)) - H(p^r(t))|$  by tracing the propagation of parameter updates through the online branch.

According to the Assumption 1, the encoder  $f$  is  $L_f$ -Lipschitz continuous w.r.t.  $\theta_f$ , we have

$$\|\mathbf{z}(t+1) - \mathbf{z}(t)\|_2 = \|f(\mathbf{x}; \theta_f(t+1)) - f(\mathbf{x}; \theta_f(t))\|_2 \leq L_f \|\theta_f(t+1) - \theta_f(t)\|. \quad (5)$$

where  $\mathbf{z} = f(\mathbf{x}; \theta_f)$  is the output feature of the encoder.

Note that in the non-collapse region  $\{p \in \Delta^{|\mathcal{C}|-1} \mid \min_c p_c \geq \delta > 0\}$ , the entropy function  $H(\cdot)$  is Lipschitz continuous with constant  $L_H = \sqrt{|\mathcal{C}|}(|\log \delta| + 1)$ , thus:

$$|H(p(t+1)) - H(p(t))| \leq L_H \|p(t+1) - p(t)\|_2. \quad (6)$$

Since the pre-trained classifier  $g$  is fixed, and the softmax function is 1-Lipschitz, combining Eqn. (5) and Eqn. (6), we have the following chain:

$$\begin{aligned} |H(p^r(t+1)) - H(p^r(t))| &\leq L_H \|p^r(t+1) - p^r(t)\|_2 \\ &\leq L_H \|g\|_2 \|\mathbf{z}^r(t+1) - \mathbf{z}^r(t)\|_2 \\ &\leq L_H \|g\|_2 L_f \|\theta_f^r(t+1) - \theta_f^r(t)\| \\ &= L_H \|g\|_2 L_f \eta_f \|\nabla_{\theta_f} H(p^o(t))\|, \end{aligned}$$

where  $\|g\|_2$  is the spectral norm of the classifier weight vector.

Let  $\phi = (\theta_h, \theta_f)$  denote the set of optimization parameters, and  $\eta_h, \eta_f$  the learning rates for the predictor and encoder. Since:

$$\begin{aligned} \eta_f &\leq \max(\eta_h, \eta_f), \\ \|\nabla_{\theta_f} H(p^o(t))\| &\leq \left\| \begin{bmatrix} \nabla_{\theta_f} H(p^o(t)) \\ \nabla_{\theta_h} H(p^o(t)) \end{bmatrix} \right\| = \|\nabla_{\phi} H(p^o(t))\|, \end{aligned}$$

we obtain:

$$\|\nabla_{\phi} H(p^o(t))\| \geq \frac{1}{L_H \|g\|_2 L_f \cdot \max(\eta_h, \eta_f)} \cdot |H(p^r(t+1)) - H(p^r(t))|. \quad \square$$

### B.3 PROOF OF LEMMA 2

**Lemma 2. (Collapse Direction with Maximal Negative Curvature)** Let  $H(\cdot)$  denote the entropy function,  $u = g(h(f(\mathbf{x}; \theta_f); \theta_h); \theta_g)$  the uncertainty logits, and  $p = \text{softmax}(u)$  the induced probability distribution. For any class  $c \in \mathcal{C}$ , there exists a direction  $\mathbf{v} = (\mathbf{v}_h, \mathbf{v}_f) \in \mathbb{R}^{\dim(\phi)}$  such that:

- (1)  $p_c$  increases monotonically along  $\mathbf{v}$ ;
- (2) As  $p_c \rightarrow 1$ , it holds that  $\mathbf{v}^\top \nabla_{\phi}^2 H \mathbf{v} \rightarrow \lambda_{\min}(\nabla_{\phi}^2 H)$ ;
- (3) For any  $\mathbf{w} \perp \mathbf{v}$ , we have  $\mathbf{v}^\top \nabla_{\phi}^2 H \mathbf{v} \leq \mathbf{w}^\top \nabla_{\phi}^2 H \mathbf{w}$ .

*Proof.* (1) Let  $\mathbf{z} = f(\mathbf{x}; \theta_f) \in \mathbb{R}^d$  be the encoder output,  $u = g(h(\mathbf{z}; \theta_h); \theta_g) \in \mathbb{R}^{|\mathcal{C}|}$  the uncertainty logits, and  $\mathbf{W}, \mathbf{P}$  the weight vector of  $g, h$ , respectively. Define  $\mathbf{v} = (\mathbf{v}_h, \mathbf{v}_f)$  such that:

$$\begin{cases} \mathbf{v}_h = a \cdot \mathbf{W}_k^\top r, \\ \mathbf{v}_f = \nabla_{\theta_f}(r^\top \mathbf{z}); \end{cases}$$

where  $r$  is a feature direction satisfying  $r^\top \mathbf{z} \neq 0$  and  $a > 0$ .  $\mathbf{v}_f$  is the direction in normalization layer parameters that amplifies the feature component along  $r$ .

This joint direction  $\mathbf{v} = (\mathbf{v}_h, \mathbf{v}_f)$  induces a change in logits:

$$\Delta u = \mathbf{W}(\mathbf{v}_h)\mathbf{z} + \mathbf{W}\mathbf{P}(\nabla_{\theta_f}\mathbf{z}\mathbf{v}_f) \approx a(r^\top \mathbf{z})\mathbf{W}\mathbf{W}_k^\top + \mathbf{W}\mathbf{P}r.$$

By choosing  $r^\top \mathbf{z} > 0$  and sufficiently large  $a$ , we ensure:

$$[\Delta u]_c > 0, \quad [\Delta u]_j = \mathcal{O}(1) \text{ for } j \neq c.$$

Thus, moving along  $\mathbf{v}$  increases  $u_c$ , and hence  $p_c = \text{softmax}(u_c)$ , monotonically.

(2) The Hessian of entropy  $H(\cdot)$  w.r.t. logits  $u$  is:

$$[\nabla_u^2 H]_{ij} = \frac{\partial^2 H}{\partial u_i \partial u_j} = p_i(\delta_{ij} - p_j)(H - \log p_i - 1).$$

As  $p_c \rightarrow 1$ , let  $\mu = 1 - p_c \rightarrow 0^+$ , and for  $p_j \approx \frac{\mu}{|\mathcal{C}|-1}$  for  $j \neq c$ . Then in the Hessian matrix

$$\begin{cases} \frac{\partial^2 H}{\partial u_c^2} = p_c(1-p_c)(H - \log p_c - 1), & \text{Diagonal for } c, \\ \frac{\partial^2 H}{\partial u_j^2} = p_j(1-p_j)(H - \log p_j - 1), & \text{Diagonal for } j \neq c, \\ \frac{\partial^2 H}{\partial u_i \partial u_j} = -p_i p_j (H - \log p_i - \log p_j - 1), & \text{Off-diagonal,} \end{cases}$$

we obtain the following approximation:

$$\begin{cases} \frac{\partial^2 H}{\partial u_c^2} \approx (1-\mu)\mu(H + \mu - 1) \approx \mu(\mu \log \frac{|\mathcal{C}|-1}{\mu} + \mu - 1) \approx -\mu, \\ \frac{\partial^2 H}{\partial u_j^2} \approx \frac{\mu}{|\mathcal{C}|-1}(\mu \log \frac{|\mathcal{C}|-1}{\mu} - \log \frac{\mu}{|\mathcal{C}|-1} - 1) \approx \frac{\mu}{|\mathcal{C}|-1} \log \frac{|\mathcal{C}|-1}{\mu} > 0, \\ \frac{\partial^2 H}{\partial u_i \partial u_j} \approx -p_i p_j (-\log p_j) > 0. \end{cases}$$

That is, as  $p_c \rightarrow 1$ , we have

$$\mathbf{v}^\top \nabla_\phi^2 H \mathbf{v} \rightarrow \lambda_{\min}(\nabla_\phi^2 H).$$

(3) The parameter space Hessian quadratic form along  $\mathbf{v}$  is:

$$\mathbf{v}^\top \nabla_\phi^2 H \mathbf{v} = \Delta u^\top \nabla_u^2 H \Delta u + \sum_i \frac{\partial H}{\partial u_i} \mathbf{v}^\top \nabla_\phi^2 u_i \mathbf{v}.$$

As  $p_c \rightarrow 1$ ,  $\nabla_u H \rightarrow 0$ , so the higher-order terms vanishes. Since  $\Delta u = \frac{\partial u}{\partial \phi} \propto e_c$ , we have:

$$\mathbf{v}^\top \nabla_\phi^2 H \mathbf{v} \propto e_c^\top \nabla_u^2 H e_c = \frac{\partial^2 H}{\partial u_c^2} < 0.$$

For any  $\mathbf{w} \perp \mathbf{v}$ ,  $\Delta u_{\mathbf{w}} = \frac{\partial u}{\partial \phi} \mathbf{w}$  is not parallel to  $e_c$ , so:

$$\mathbf{w}^\top \nabla_\phi^2 H \mathbf{w} \geq \mathbf{v}^\top \nabla_\phi^2 H \mathbf{v}.$$

□

#### B.4 PROOF OF THEOREM 1

**Theorem 1. (Optimization and Stability of ZeroSiam)** Consider the ZeroSiam objective  $\mathcal{L} = H(p^o) + \alpha D(p^o \| \text{sg}[p^r])$ , where  $H(\cdot)$  denotes the entropy loss,  $D(\cdot)$  the alignment regularizer, and  $p^o, p^r \in \Delta^{|\mathcal{C}|-1}$  are the probability distributions induced by the online and target branches. Given the encoder  $f$ , classifier  $g$  and predictor  $h$ . Under Assumptions 1 and 2, the following hold:

(1) For  $\alpha = 0$ , the entropy variation satisfies  $|\Delta H(p^o)| > |\Delta H(p^r)|$ , and the Hessian of  $H(p^o)$  attains its minimal eigenvalue along collapse directions  $\mathbf{v}$ :

$$\lambda_{\min}(\nabla^2 H(p^o)) = \mathbf{v}^\top \nabla^2 H(p^o) \mathbf{v}.$$

(2) For  $\alpha > 0$ , the predictor  $h$  serves as a filtering mechanism that suppresses gradient update directions corresponding to over-amplified logits, and the system converges to a stable equilibrium: there exists  $h_{\min} > 0$  such that

$$H(p^o) > h_{\min}, \quad p^o \rightarrow p^r.$$

*Proof.* (1) By Lemma 1, the target branch entropy variation is determined by the gradient of the online branch:

$$\|\nabla_\phi H(p^o(t))\| \geq \frac{1}{L \cdot \eta_{\max}} \cdot |H(p^r(t+1)) - H(p^r(t))|, \quad (7)$$

where  $L = L_H \|g\|_2 L_f$  and  $\eta_{\max} = \max(\eta_h, \eta_f)$ .

Under the Assumption 2 that  $\mathcal{L} = H(\cdot)$  is  $\rho$ -smoothness and  $\eta_{\max} < \frac{1}{\rho}$ , the descent lemma gives:

$$H(p^o(t+1)) \leq H(p^o(t)) - \nabla_\phi H^\top D_\eta \nabla_\phi H + \frac{\rho}{2} \|D_\eta \nabla_\phi H\|^2,$$

where  $D_\eta = \text{diag}(\eta_f \mathbf{I}_{d_f}, \eta_h \mathbf{I}_{d_h})$ . So we have:

$$|\Delta H^o| = H(p^o(t+1)) - H(p^o(t)) \geq \eta_{\min} \|\nabla_\phi H\|^2, \quad \eta_{\min} = \min(\eta_h, \eta_f). \quad (8)$$

Combining Eqn. (7) and Eqn. (8), we obtain:

$$\frac{|\Delta H^o|}{|\Delta H^r|} \geq \frac{\eta_{\min} \|\nabla_\phi H\|^2}{L \cdot \eta_{\max} \|\nabla_\phi H\|} = \frac{\eta_{\min}}{\eta_{\max}} \cdot \frac{\|\nabla_\phi H\|}{L}.$$

Since  $L, \|\nabla_\phi H\| > 0$  and bounded in non-collapse regions, achieving  $\frac{|\Delta H^o|}{|\Delta H^r|} > 1$  requires:

$$\frac{\eta_{\min}}{\eta_{\max}} > \frac{L}{\|\nabla_\phi H\|}.$$

In practice, we set  $\eta_h = k \cdot \eta_f$  with  $k > 1$ , so there always exists a  $k$  such that

$$|\Delta H(p^o)| > |\Delta H(p^r)|.$$

We further construct the direction  $\mathbf{v} = (\mathbf{v}_h, \mathbf{v}_f) \in \mathbb{R}^{\dim(\phi)}$  according to Lemma 2, the corresponding directional derivative is given by:

$$D_{\mathbf{v}} H = \nabla_\phi H^\top \mathbf{v} \propto [\nabla_u H]_c,$$

where  $u$  is the uncertainty logits. And the second-order directional derivative is:

$$D_{\mathbf{v}}^2 H = \mathbf{v}^\top \nabla_\phi^2 H \mathbf{v} = \lambda_{\min} < 0.$$

This implies that along  $\mathbf{v}$ , the loss decreases fastest at second order (Jin et al., 2017).

Moreover, by Lemma 2,  $p_c$  increases monotonically along  $\mathbf{v}$ , thus  $[\nabla_u H]_c = p_c(H - \log p_c - 1)$  increases synchronously, creating a self-reinforcing feedback loop that accelerates collapse.

(2) Consider the optimization objective:

$$\mathcal{L} = H(p^o) + \alpha D(p^o \parallel \text{sg}[p^r]),$$

where  $D(p^o \parallel \text{sg}[p^r]) = D_{\text{KL}}(p^o \parallel \text{sg}[p^r]) + D_{\text{KL}}(\text{sg}[p^r] \parallel p^o)$  are symmetric KL loss.

Under the stop-gradient setting on the target branch, the gradient of the shared encoder  $f$  is solely determined by the online branch. We have:

$$\nabla_{\mathbf{z}} \mathcal{L} = \left( \frac{\partial u^o}{\partial \mathbf{z}} \right) \nabla_{u^o} \mathcal{L} = \mathbf{P}^\top \mathbf{W}^\top [\nabla_{u^o} H(p^o) + 2\alpha(p^o - p^r)],$$

where  $\mathbf{z} = f(\mathbf{x}; \theta_f)$  is the encoder output,  $\mathbf{W}, \mathbf{P}$  the weight vector of the classifier  $g$  and the predictor  $h$ , respectively. Consider a parameter update unit direction  $\mathbf{v}_h$ ,  $\|\mathbf{v}_h\|_2 = 1$ , then:

$$\langle \nabla_{\mathbf{z}} \mathcal{L}, \mathbf{v}_h \rangle = \mathbf{v}_h^\top \nabla_{\mathbf{z}} \mathcal{L} = \mathbf{v}_h^\top \left( \frac{\partial u^o}{\partial \mathbf{z}} \right) \nabla_{u^o} \mathcal{L} = \mathbf{P}^\top \mathbf{W}^\top [\nabla_{u^o} H(p^o) + 2\alpha(p^o - p^r)]$$

During the minimization of  $\mathcal{L}$ , the predictor  $h$  encourages the update direction that ensuring

$$p^o \rightarrow p^r,$$

and suppresses gradient update directions corresponding to over-amplified logits.

We further analyze the convergence properties of the optimization system.

By the definition of entropy and KL divergence, we have:

$$H(p^o) = - \sum_{c=1}^{|C|} p_c^o \log p_c^o = - \sum_{c=1}^{|C|} p_c^o \log p_c^r - D_{\text{KL}}(p^o \parallel p^r).$$

Applying Gibbs' inequality,  $-\sum_{c=1}^{|C|} p_c^o \log p_c^r \geq H(p^r)$ , we obtain:

$$H(p^o) \geq H(p^r) - D_{\text{KL}}(p^o \parallel p^r).$$

Since  $D_{\text{SKL}}(p^o \parallel p^r) \geq D_{\text{KL}}(p^o \parallel p^r)$ , it follows that:

$$H(p^o) \geq H(p^r) - D_{\text{SKL}}(p^o \parallel p^r). \quad (9)$$

When the target branch is still in the non-collapse region  $\{p^r \in \Delta^{|\mathcal{C}|-1} \mid \min_c p_c^r \geq \delta > 0\}$ , the entropy satisfies:

$$H(p^r) \geq -\log(1 - (1 - |\mathcal{C}|)\delta) > 0. \quad (10)$$

Define the Lyapunov function  $V(t) = \mathcal{L}(t)$ . Since  $H(p^o) \geq 0$  and  $D_{\text{SKL}}(p^o || p^r) \geq 0$ , we have

$$V(t) > 0.$$

Moreover, under the Assumption 2, the descent lemma guarantees:

$$V(t+1) \geq V(t) - \frac{\eta_{\min}}{2} \|\nabla_{\phi} \mathcal{L}(t)\|^2 \leq V(t).$$

Thus,  $V(t)$  is monotonically decreasing and bounded below. According to the Monotone Convergence Theorem,  $V(t) \rightarrow V^* > 0$ . In particular:

$$D_{\text{SKL}}(p^o(t) || p^r(t)) \leq \frac{V(0)}{\alpha}. \quad (11)$$

Combining Eqn. (9), Eqn. (10), and Eqn. (11):

$$H(p^o) \geq H(p^r) - D_{\text{SKL}}(p^o || p^r) \geq -\log(1 - (1 - |\mathcal{C}|)\delta) - \frac{V(0)}{\alpha}.$$

Define

$$h_{\min} = -\log(1 - (1 - |\mathcal{C}|)\delta) - \frac{V(0)}{\alpha}.$$

Let the hyperparameter  $\alpha > \frac{V(0)}{-\log(1 - (1 - |\mathcal{C}|)\delta)}$ , then  $h_{\min} > 0$ .

Overall, we have proven that the predictor  $h$  serves as a filtering mechanism that suppresses gradient update directions corresponding to over-amplified logits, and the system converges to a stable equilibrium: there exists  $h_{\min} > 0$  such that

$$H(p^o) > h_{\min}, \quad p^o \rightarrow p^r.$$

□

## C MORE IMPLEMENTATION DETAILS

### C.1 MORE DETAILS ON DATASET

For vision adaptation, we evaluate the out-of-distribution generalization ability of all methods on a large-scale and widely used benchmark, namely **ImageNet-C**<sup>2</sup> (Hendrycks & Dietterich, 2019). ImageNet-C is constructed by corrupting the original ImageNet (Deng et al., 2009) test set. The corruption (as shown in Figure A) consists of 15 different types, *i.e.*, Gaussian noise, shot noise, impulse noise, defocus blur, glass blur, motion blur, zoom blur, snow, frost, fog, brightness, contrast, elastic transformation, pixelation, and JPEG compression, where each corruption type has 5 severity levels and the larger severity level means more severe distribution shift.

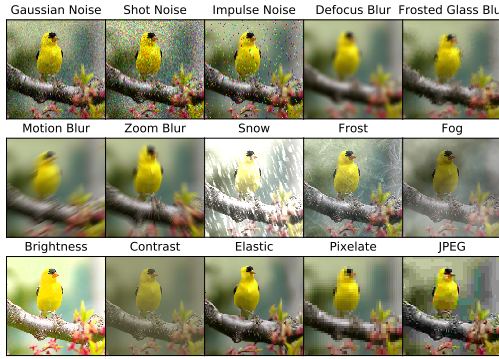


Figure A: Visualizations of different corruption types in ImageNet-C benchmark.

For natural language reasoning, we evaluate the effectiveness of online reasoning incentivization on a comprehensive mathematical reasoning benchmark, including Math-500 (Lightman et al., 2023), CollegeMath (Tang et al., 2024), AIME24 (Codeforces, 2024), and Minerva (Lewkowycz et al., 2022). Specifically, Math-500 is derived from the larger MATH benchmark (Hendrycks et al., 2021), consisting of difficult mathematics problems originally taken from high school competitions. It spans domains such as pre-algebra, algebra, number theory, and calculus, emphasizing abstract reasoning and multi-step problem solving. CollegeMath is a college-level mathematics dataset constructed from nine open-access college textbooks, covering seven core areas: algebra, pre-calculus, calculus, vector calculus, probability, linear algebra, and differential equations. The full dataset contains 2818 test questions, from which we sample 1200 for efficient evaluation. AIME24 consists of 30 advanced problems from the 2024 American Invitational Mathematics Examination (AIME) I and II, designed to test extended chain-of-thought reasoning. Minerva includes 272 undergraduate-level mathematics and science questions from MIT OpenCourseWare (OCW), aimed at assessing models' reasoning ability in scientific problem-solving contexts.

### C.2 MORE EXPERIMENTAL PROTOCOLS

All pre-trained models involved in our paper are publicly available, including ResNet50-GN<sup>3</sup>, ViT-Base<sup>4</sup>, ViT-Small<sup>5</sup>, ConvNeXt-Tiny<sup>6</sup> and Swin-Tiny<sup>7</sup> obtained from `timm` repository (Wightman,

<sup>2</sup><https://zenodo.org/record/2235448#.YzQpq-xBxcA>

<sup>3</sup>[https://github.com/rwightman/pytorch-image-models/releases/download/v0.1-rsb-weights/resnet50\\_gn\\_a1h2-8fe6c4d0.pth](https://github.com/rwightman/pytorch-image-models/releases/download/v0.1-rsb-weights/resnet50_gn_a1h2-8fe6c4d0.pth)

<sup>4</sup>[https://storage.googleapis.com/vit\\_models/augreg/B\\_16-i21k-300ep-lr\\_0.001-aug\\_medium1-wd\\_0.1-do\\_0.0-sd\\_0.0--imagenet2012-steps\\_20k-lr\\_0.01-res\\_224.npz](https://storage.googleapis.com/vit_models/augreg/B_16-i21k-300ep-lr_0.001-aug_medium1-wd_0.1-do_0.0-sd_0.0--imagenet2012-steps_20k-lr_0.01-res_224.npz)

<sup>5</sup>[https://storage.googleapis.com/vit\\_models/augreg/S\\_16-i21k-300ep-lr\\_0.001-aug\\_light1-wd\\_0.03-do\\_0.0-sd\\_0.0--imagenet2012-steps\\_20k-lr\\_0.03-res\\_224.npz](https://storage.googleapis.com/vit_models/augreg/S_16-i21k-300ep-lr_0.001-aug_light1-wd_0.03-do_0.0-sd_0.0--imagenet2012-steps_20k-lr_0.03-res_224.npz)

<sup>6</sup>[https://github.com/rwightman/pytorch-image-models/releases/download/v0.1-rsb-weights/convnext\\_tiny\\_hnf\\_a2h-ab7e9df2.pth](https://github.com/rwightman/pytorch-image-models/releases/download/v0.1-rsb-weights/convnext_tiny_hnf_a2h-ab7e9df2.pth)

<sup>7</sup>[https://github.com/SwinTransformer/storage/releases/download/v1.0.0/swin\\_tiny\\_patch4\\_window7\\_224.pth](https://github.com/SwinTransformer/storage/releases/download/v1.0.0/swin_tiny_patch4_window7_224.pth)

2019) for image classification, and Llama3.1-8B-Instruct<sup>8</sup> (Dubey et al., 2024) for natural language reasoning. In the following, we provide the implementation details of our proposed method and all comparative methods evaluated in our experiments, which help reproduce our results.

**ZeroSiam (Ours).** We use symmetric KL as the divergence term in Eqn. (4), and  $\alpha$  is fixed to 1 without tuning. For vision adaptation, we use SGD as the update rule, with a momentum of 0.9, batch size of 64 (except for the experiments of batch size = 1), learning rate  $\eta_f$  of 0.0025 / 0.005 / 0.001 / 0.00025 / 0.0005 with learning rate  $\eta_h$  of 0.025 / 0.005 / 0.01 / 0.0025 / 0.0025 for ResNet50-GN / ViT-Base / ViT-Small / ConvNeXt-Tiny / Swin-Tiny, respectively. The learning rate for batch size = 1 is scaled down by 16 for ResNet50-GN and 32 for other models following SAR. The trainable parameters are all the affine parameters of normalization layers. For natural language reasoning, following the configuration for TLM, we use AdamW as the update rule, with  $\beta_1 = 0.9$ ,  $\beta_2 = 0.999$ , weight decay = 0.0, and optimize the prediction entropy of the first 8 output tokens. Both learning rates  $\eta_f$  and  $\eta_h$  are set to  $7.5 \times 10^{-6}$  /  $5 \times 10^{-6}$  /  $1.25 \times 10^{-5}$  /  $5 \times 10^{-6}$  for Math-500 / CollegeMath / AIME24 / Minerva. Trainable parameters are the LoRA parameters with a rank of 8.

**Tent<sup>9</sup> (Wang et al., 2021).** We follow all hyper-parameters that are set in Tent unless it does not provide. Specifically, for vision adaptation, we use SGD as the update rule, with a momentum of 0.9, batch size of 64 (except for the experiments of batch size = 1), and learning rate of 0.00025 / 0.001 / 0.0001 / 0.000025 / 0.00005 for ResNet50-GN / ViT-Base / ViT-Small / ConvNeXt-Tiny / Swin-Tiny, respectively. The learning rate for batch size = 1 is scaled down to (0.00025/32) for ResNet50-GN, (0.001/64) for ViT-Base, (0.0001/64) for ViT-Small, (0.000025/64) for ConvNeXt-Tiny and (0.00005/64) for Swin-Tiny. The trainable parameters are all the affine parameters of normalization layers. For natural language reasoning, we use AdamW as the update rule, with  $\beta_1 = 0.9$ ,  $\beta_2 = 0.999$ , weight decay = 0.0, and optimize the prediction entropy of the first 8 output tokens. The learning rate is  $7.5 \times 10^{-6}$  /  $5 \times 10^{-6}$  /  $1.25 \times 10^{-5}$  /  $5 \times 10^{-6}$  for Math-500 / CollegeMath / AIME24 / Minerva. The trainable parameters are the LoRA parameters with a rank of 8.

**SAR<sup>10</sup> (Niu et al., 2023).** We follow all hyper-parameters that are set in SAR unless it does not provide. Specifically, for vision adaptation, we use SGD as the update rule, with a momentum of 0.9, batch size of 64 (except for the experiments of batch size = 1), and learning rate of 0.00025 / 0.001 / 0.0001 / 0.000025 / 0.00005 for ResNet50-GN / ViT-Base / ViT-Small / ConvNeXt-Tiny / Swin-Tiny. The learning rate for batch size = 1 is scaled down to (0.00025/16) for ResNet50-GN, (0.001/32) for ViT-Base, (0.0001/32) for ViT-Small, (0.000025/32) for ConvNeXt-Tiny and (0.00005/32) for Swin-Tiny. The entropy threshold  $E_0$  is set to  $0.4 \times \ln C$ , where  $C$  is the number of task classes. The trainable parameters are the affine parameters of norm layers from layer 1 to layer 3 in ResNet50-GN, from blocks 1 to blocks 8 in ViT-Base and ViT-Small, and all affine parameters in other models. For natural language reasoning,  $E_0$  is set to 0.4. We use AdamW as the update rule, with  $\beta_1 = 0.9$ ,  $\beta_2 = 0.999$ , weight decay = 0.0, and optimize the prediction entropy of the first 8 output tokens. The learning rate is  $7.5 \times 10^{-6}$  /  $5 \times 10^{-6}$  /  $1.25 \times 10^{-5}$  /  $5 \times 10^{-6}$  for Math-500 / CollegeMath / AIME24 / Minerva, trainable parameters are the LoRA parameters with a rank of 8.

**EATA<sup>11</sup> (Niu et al., 2022).** We follow all hyper-parameters that are set in EATA unless it does not provide. Specifically, for vision adaptation, the entropy constant  $E_0$  (for reliable sample identification) is set to  $0.4 \times \ln C$ , where  $C$  is the number of task classes. The  $\epsilon$  for redundant sample identification is set to 0.05. The trade-off parameter  $\beta$  for entropy loss and regularization loss is set to 2,000. The number of pre-collected in-distribution test samples for Fisher importance calculation is 2,000. The update rule is SGD, with a momentum of 0.9, batch size of 64 (except for the experiments of batch size = 1), and learning rate of 0.00025 / 0.001 / 0.0001 / 0.000025 / 0.00005 for ResNet50-GN / ViT-Base / ViT-Small / ConvNeXt-Tiny / Swin-Tiny. The learning rate for batch size = 1 is scaled down to (0.00025/32) for ResNet50-GN, (0.001/64) for ViT-Base, (0.0001/64) for ViT-Small, (0.000025/64) for ConvNeXt-Tiny and (0.00005/64) for Swin-Tiny. The trainable parameters are all affine parameters of normalization layers. For natural language reasoning,  $E_0$  is set to 0.4, while the anti-forgetting regularizer is not applied due to a lack of knowledge for in-distribution data that the large language model trains on. We use AdamW as the update rule, with  $\beta_1 = 0.9$ ,  $\beta_2 = 0.999$ , weight decay = 0.0, and optimize the prediction entropy of the first 8 output tokens. The

<sup>8</sup><https://huggingface.co/meta-llama/Llama-3.1-8B-Instruct>

<sup>9</sup><https://github.com/DequanWang/tent>

<sup>10</sup><https://github.com/mr-eggplant/SAR>

<sup>11</sup><https://github.com/mr-eggplant/EATA>

learning rate is  $7.5 \times 10^{-6} / 5 \times 10^{-6} / 1.25 \times 10^{-5} / 5 \times 10^{-6}$  for Math-500 / CollegeMath / AIME24 / Minerva. The trainable parameters are the LoRA parameters with a rank of 8.

**DeYO<sup>12</sup> (Lee et al., 2024).** We follow all hyper-parameters that are set in DeYO unless it does not provide. Specifically, the entropy constant  $E_0$  (for reliable sample identification) is set to  $0.4 \times \ln 1000$ , and the factor  $\tau_{\text{Ent}}$  is set to  $0.5 \times \ln 1000$ . The Pseudo-Label Probability Difference (PLPD) threshold  $\tau_{\text{PLPD}}$  is set to 0.2. The update rule is SGD, with a momentum of 0.9, batch size of 64 (except for the experiments of batch size = 1), and learning rate of  $0.00025 / 0.001 / 0.0001 / 0.000025 / 0.00005$  for ResNet50-GN / ViT-Base / ViT-Small / ConvNeXt-Tiny / Swin-Tiny. The learning rate for batch size = 1 is scaled down to (0.00025/16) for ResNet50-GN, (0.001/32) for ViT-Base, (0.0001/32) for ViT-Small, (0.000025/32) for ConvNeXt-Tiny and (0.00005/32) for Swin-Tiny. Trainable parameters are the affine parameters of norm layers from layer 1 to 3 in ResNet50-GN, from blocks 1 to 8 in ViT-Base and ViT-Small, and all affine parameters in other models.

**COME<sup>13</sup> (Zhang et al., 2025).** For vision adaptation, we implement COME based on DeYO for comparisons, following the hyper-parameters set in DeYO unless otherwise specified. Specifically, the entropy constant  $E_0$  (for reliable sample identification) is set to  $0.4 \times \ln 1000$ , and the factor  $\tau_{\text{Ent}}$  is set to  $0.5 \times \ln 1000$ . The Pseudo-Label Probability Difference (PLPD) threshold  $\tau_{\text{PLPD}}$  is set to 0.2. The uncertainty mass is set to  $C$ , where  $C$  is the number of task classes. The update rule is SGD, with a momentum of 0.9, batch size of 64 (except for the experiments of batch size = 1), and learning rate of  $0.00025 / 0.001 / 0.0001 / 0.000025 / 0.00005$  for ResNet50-GN / ViT-Base / ViT-Small / ConvNeXt-Tiny / Swin-Tiny. The learning rate for batch size = 1 is scaled down to (0.00025/16) for ResNet50-GN, (0.001/32) for ViT-Base, (0.0001/32) for ViT-Small, (0.000025/32) for ConvNeXt-Tiny and (0.00005/32) for Swin-Tiny. The trainable parameters are the affine parameters of norm layers from layer 1 to layer 3 in ResNet50-GN, from blocks 1 to blocks 8 in ViT-Base and ViT-Small, and all affine parameters in other models. For natural language reasoning, COME is implemented based on Tent, and uncertainty mass is set to  $|Z|$ , where  $|Z|$  denotes the vocabulary size. We use AdamW as the update rule, with  $\beta_1 = 0.9$ ,  $\beta_2 = 0.999$ , weight decay = 0.0, and optimize the prediction entropy of the first 8 output tokens. The learning rate is  $7.5 \times 10^{-6} / 5 \times 10^{-6} / 1.25 \times 10^{-5} / 5 \times 10^{-6}$  for Math-500 / CollegeMath / AIME24 / Minerva. The trainable parameters are the LoRA parameters with a rank of 8.

**TLM (Hu et al., 2025a)<sup>14</sup>.** We follow all hyper-parameters that are set in TLM unless it does not provide. Specifically, we compare with TLM on the natural language reasoning task, the perplexity threshold  $\mathcal{P}$ , is set to  $e^3$ . The update rule is AdamW, with  $\beta_1 = 0.9$ ,  $\beta_2 = 0.999$ , weight decay = 0.0. The learning rate is  $7.5 \times 10^{-6} / 5 \times 10^{-6} / 1.25 \times 10^{-5} / 5 \times 10^{-6}$  for Math-500 / CollegeMath / AIME24 / Minerva. The trainable parameters are the LoRA parameters with a rank of 8.

<sup>12</sup><https://github.com/Jhyun17/DeYO>

<sup>13</sup><https://github.com/BlueWhaleLab/COME>

<sup>14</sup><https://github.com/Fhujinwu/TLM>

## D MORE EXPERIMENTAL RESULTS

In this section, we provide the detailed results of Tables 3-6 in the main paper and include additional experiments under both mild and wild testing scenarios to enable a comprehensive comparison.

### D.1 DETAILED AND ADDITIONAL RESULTS UNDER WILD TEST SCENARIOS

We first provide the detailed results of TTA under label shifts and a single sample. From Tables A & B, ZeroSiam achieves superior performance across nearly all cases, *e.g.*, 51.6% (Ours) *vs.* 43.9% (DeYO) on ResNet50-GN under label shifts, and 51.3% (Ours) *vs.* 42.3% (COME) on ViT-Small under the batch size of 1. Similar results are observed even when the data stream exhibits both label shifts and data scarcity, as shown in Table C, suggesting our effectiveness across test settings.

### D.2 DETAILED RESULTS FOR TTA ON THE BLIND-SPOT SUBSET

From Table D, prior methods tend to collapse when adapting on the blind-spot subset, *e.g.*, 18.9% (DeYO) *vs.* 30.6% (NoAdapt) w.r.t. the average accuracy on R50-GN. In contrast, even under such a challenging setting, ZeroSiam achieves consistent improvement across all domains and models, suggesting that ZeroSiam substantially expands the scope and reliability of TTA in the real world.

### D.3 DETAILED RESULTS UNDER THE MILD TEST SCENARIO

ZeroSiam is not only effective under challenging test scenarios, but also enhances TTA performance significantly on the mild test scenario (Wang et al., 2021), where data comes with shuffled labels. As shown in Table E, ZeroSiam demonstrates superior performance on 4 out of 5 models and also achieves comparative results on ViT-Base, *e.g.*, the average accuracy of 48.6% (Ours) *vs.* 41.7% (DeYO) on ResNet50-GN, and 62.6% (Ours) *vs.* 62.8% (DeYO) on ViT-Base. This suggests that our ZeroSiam’s design helps improve the stability and efficacy of TTA across a wide range of scenarios.

Table A: Detailed results of TTA under **IMBALANCED LABEL SHIFTS**, Table 3 in the main paper.

Model+Method	Noise			Blur			Weather			Digital			Avg.			
	Gauss.	Shot	Impul.	Defoc.	Glass	Motion	Zoom	Snow	Frost	Fog	Brit.	Contr.	Elastic	Pixel	JPEG	
ResNet50-GN	18.0	19.8	17.9	19.8	11.4	21.4	24.9	40.4	47.3	33.6	69.3	36.3	18.6	28.4	52.3	30.6
• Tent	2.6	3.3	2.7	13.9	7.9	19.5	17.0	16.5	21.9	1.8	70.5	42.2	6.6	49.4	53.7	22.0
• SAR	33.1	36.5	35.5	19.2	19.5	33.3	27.7	23.9	45.3	50.1	71.9	46.7	7.1	52.1	56.3	37.2
• EATA	27.0	28.3	28.1	14.9	17.1	24.4	25.3	32.2	32.0	39.8	66.7	33.6	24.5	41.9	38.4	31.6
• COME	17.7	19.7	17.7	19.7	11.2	21.2	24.8	40.2	47.8	33.7	68.9	35.6	18.6	27.7	51.8	30.4
• DeYO	42.5	44.9	43.8	22.2	16.3	41.0	13.2	52.2	51.5	39.7	73.4	52.6	46.9	59.3	59.3	43.9
• ZeroSiam (ours)	42.9	45.1	43.1	35.1	36.1	44.5	49.2	58.1	55.1	62.9	72.3	54.8	52.5	61.7	60.1	<b>51.6</b>
ViT-Base	9.4	6.7	8.3	29.1	23.4	34.0	27.0	15.8	26.3	47.4	54.7	43.9	30.5	44.5	47.6	29.9
• Tent	32.7	1.4	34.6	54.4	52.3	58.2	52.2	7.7	12.0	69.3	76.1	66.1	56.7	69.4	66.4	47.3
• SAR	46.5	43.1	48.9	55.3	54.3	58.9	54.8	53.6	46.2	69.7	76.2	66.2	60.9	69.6	66.6	58.0
• EATA	35.9	34.6	36.7	45.3	47.2	49.3	47.7	56.5	55.4	62.2	72.2	21.7	56.2	64.7	63.7	50.0
• COME	45.3	52.1	52.0	56.1	57.4	62.5	60.7	66.6	64.0	71.6	77.1	65.9	61.9	72.9	69.2	62.4
• DeYO	53.5	36.0	54.6	57.6	58.7	63.7	46.2	67.6	66.0	73.2	77.9	66.7	69.0	73.5	70.3	62.3
• ZeroSiam (ours)	52.3	52.6	53.4	57.7	58.7	62.7	61.1	67.6	66.0	73.3	78.0	67.0	67.9	73.5	70.1	<b>64.1</b>
ViT-Small	2.0	2.0	1.5	24.2	17.1	30.3	22.0	9.5	19.2	37.9	44.4	30.1	24.8	38.2	41.0	22.9
• Tent	0.3	0.4	0.2	43.1	37.0	45.4	36.3	5.5	24.2	58.4	65.8	54.6	26.6	56.6	54.9	34.0
• SAR	1.6	2.0	1.3	44.3	39.0	46.5	39.0	16.6	45.9	58.6	65.8	54.7	44.4	56.9	55.2	38.1
• EATA	15.6	15.5	17.8	42.4	40.3	44.8	41.6	46.2	48.7	58.9	65.3	52.9	50.5	57.2	56.2	43.6
• COME	0.1	0.2	0.1	47.4	47.2	52.8	10.5	35.5	53.8	63.9	70.7	58.1	56.7	63.4	60.2	41.4
• DeYO	0.1	0.2	0.1	48.4	47.7	53.4	16.2	47.0	54.6	65.0	71.0	59.3	58.5	64.1	61.0	43.1
• ZeroSiam (ours)	25.7	25.9	27.9	48.2	48.3	53.5	51.5	55.7	55.6	65.4	71.2	58.4	59.5	64.2	61.2	<b>51.5</b>
ConvNeXt-Tiny	21.4	27.7	22.1	24.5	11.0	32.5	31.2	44.5	52.5	39.5	72.0	44.8	23.1	17.7	55.8	34.7
• Tent	18.1	23.8	26.6	24.3	4.2	33.9	29.2	41.6	46.3	39.7	73.2	51.6	18.4	10.7	56.9	33.2
• SAR	34.8	36.7	34.9	27.1	4.1	35.0	30.8	44.3	47.6	8.4	73.1	51.1	19.4	24.7	56.7	35.2
• EATA	34.4	36.8	35.0	26.7	19.1	37.0	33.3	47.7	48.4	50.6	73.0	51.9	28.7	31.4	56.9	40.7
• COME	42.6	44.5	42.4	38.7	1.2	46.0	11.8	57.1	56.9	61.8	75.6	60.6	5.3	51.9	61.9	43.9
• DeYO	33.2	38.0	36.7	27.9	2.6	36.4	9.2	52.7	45.3	2.9	74.4	56.6	4.7	19.5	58.4	33.2
• ZeroSiam (ours)	42.3	44.5	42.1	37.4	33.5	45.3	44.0	56.5	55.4	62.9	74.7	59.4	44.3	51.7	60.0	<b>50.3</b>
Swin-Tiny	26.6	27.9	22.8	21.7	13.2	26.5	25.4	41.0	45.8	47.7	67.6	39.1	22.6	8.4	33.3	31.3
• Tent	16.1	14.1	10.5	17.1	16.9	23.5	20.0	30.4	28.3	11.3	69.7	47.8	9.3	1.1	43.2	24.0
• SAR	29.8	28.0	29.8	19.8	10.6	24.4	21.2	33.1	34.3	22.3	67.9	45.9	13.2	4.8	42.9	28.5
• EATA	36.2	37.1	33.6	26.3	29.8	38.2	37.3	47.3	44.5	51.4	70.3	42.4	40.9	34.8	46.5	41.1
• COME	41.8	43.6	43.2	36.5	9.8	46.7	2.4	54.6	52.3	60.0	72.0	47.4	4.3	3.1	55.8	38.2
• DeYO	40.1	43.3	42.4	20.9	32.0	42.2	12.3	49.4	49.0	55.7	72.3	53.3	38.5	42.1	53.3	43.1
• ZeroSiam (ours)	44.4	45.8	45.7	36.4	38.3	47.0	47.0	54.3	51.9	58.7	72.4	54.2	52.7	51.8	55.5	<b>50.4</b>

Table B: Detailed results of TTA with **BATCH SIZE=1**, i.e., Table 4 in the main paper.

Model+Method	Noise			Blur			Weather				Digital			Avg.		
	Gauss.	Shot	Impul.	Defoc.	Glass	Motion	Zoom	Snow	Frost	Fog	Brit.	Contr.	Elastic	Pixel	JPEG	
ResNet50-GN	18.0	19.8	17.9	19.8	11.4	21.4	24.9	40.4	47.3	33.6	69.3	36.3	18.6	28.4	52.3	30.6
• Tent	2.5	2.9	2.5	13.5	3.6	18.6	17.6	15.3	23.0	1.4	70.4	42.2	6.2	49.2	53.8	21.5
• SAR	23.4	26.6	23.0	18.4	15.4	28.6	30.4	44.9	44.7	25.7	72.3	44.5	14.8	47.0	56.1	34.5
• EATA	24.8	28.3	25.7	18.1	17.3	28.5	29.3	44.5	44.3	41.6	70.9	44.6	27.0	46.8	55.7	36.5
• COME	17.8	19.7	17.7	19.7	11.3	21.4	24.9	40.3	47.6	33.6	68.9	35.7	18.5	27.9	51.8	30.5
• DeYO	41.8	44.7	43.0	22.5	24.7	41.8	24.4	54.5	52.2	20.7	73.5	53.5	48.5	60.2	59.8	44.4
• ZeroSiam (ours)	41.7	44.4	41.8	32.8	35.8	45.2	49.5	58.4	55.5	63.8	73.7	54.8	55.1	63.6	61.0	<b>51.8</b>
ViT-Base	9.5	6.7	8.2	29.0	23.4	33.9	27.1	15.9	26.5	47.2	54.7	44.1	30.5	44.5	47.8	29.9
• Tent	42.2	1.0	43.3	52.4	48.2	55.5	50.5	16.5	16.9	66.4	74.9	64.7	51.6	67.0	64.3	47.7
• SAR	40.8	36.4	41.5	53.7	50.7	57.5	52.8	59.1	50.7	68.1	74.6	65.7	57.9	68.9	65.9	56.3
• EATA	29.7	25.1	34.6	44.7	39.2	48.3	42.4	37.5	45.9	60.0	65.9	61.2	46.4	58.2	59.6	46.6
• COME	51.7	51.4	52.1	57.6	58.2	63.3	41.2	67.1	64.8	72.8	77.7	68.1	67.5	73.0	69.9	62.4
• DeYO	54.0	52.1	55.1	58.8	59.5	64.2	53.5	68.2	66.4	73.7	78.3	68.2	68.9	73.8	70.8	<b>64.4</b>
• ZeroSiam (ours)	52.1	52.7	52.8	57.8	58.3	63.0	60.6	67.0	65.7	73.0	77.9	67.6	67.9	72.8	69.9	63.9
ViT-Small	2.0	1.9	1.5	24.3	17.1	30.2	21.8	9.5	19.3	37.9	44.4	29.9	24.9	38.2	41.3	22.9
• Tent	21.3	27.7	22.0	24.5	10.6	32.3	30.9	44.6	52.4	39.6	72.3	44.5	23.4	17.6	55.6	34.6
• SAR	26.9	27.7	23.0	21.7	13.2	26.4	25.3	41.2	45.8	47.7	67.8	39.2	22.5	8.4	33.2	31.3
• EATA	2.4	2.5	1.8	32.8	25.4	36.3	28.2	17.1	28.2	48.7	53.5	46.1	34.1	46.7	47.7	30.1
• COME	0.5	3.5	0.4	48.4	47.3	52.9	15.4	38.2	53.8	64.3	70.7	58.8	55.8	63.6	60.4	42.3
• DeYO	0.4	0.8	0.3	49.0	47.4	53.0	20.1	46.4	54.6	64.7	70.9	59.3	57.3	64.1	61.0	43.3
• ZeroSiam (ours)	26.0	26.9	28.3	48.6	48.2	52.7	50.7	54.4	55.1	65.0	71.0	59.1	58.6	63.4	60.8	<b>51.3</b>
ConvNeXt-Tiny	21.3	27.7	22.0	24.5	10.6	32.3	30.9	44.6	52.4	39.6	72.3	44.5	23.4	17.6	55.6	34.6
• Tent	30.3	33.5	32.0	24.7	7.3	33.6	30.0	43.7	47.3	43.7	72.9	49.7	21.4	18.5	56.3	36.3
• SAR	30.3	33.6	29.8	25.9	11.1	33.4	30.8	44.9	47.8	38.3	72.9	46.2	22.6	18.1	56.2	36.1
• EATA	26.6	30.5	26.9	25.2	11.4	33.1	31.0	44.8	50.1	40.0	72.2	47.8	23.5	18.5	55.8	35.8
• COME	41.1	43.2	41.1	37.3	2.1	44.5	17.9	56.4	55.8	60.7	75.2	59.6	8.6	44.7	61.1	43.3
• DeYO	36.8	39.4	37.0	29.5	2.9	38.0	14.6	51.6	46.9	4.5	74.0	55.9	7.8	19.5	57.9	34.4
• ZeroSiam (ours)	41.5	43.6	41.5	37.2	32.5	44.8	42.7	55.6	54.7	62.2	74.3	59.0	42.3	50.5	59.3	<b>49.4</b>
Swin-Tiny	26.9	27.7	23.0	21.7	13.2	26.4	25.3	41.2	45.8	47.7	67.8	39.2	22.5	8.4	33.2	31.3
• Tent	23.8	26.2	22.5	19.4	18.4	26.9	27.3	40.4	36.0	22.8	69.2	46.5	16.5	2.4	41.4	29.3
• SAR	25.4	27.1	23.0	21.6	14.8	27.3	27.5	38.9	37.5	44.1	67.7	38.4	18.9	8.3	39.5	30.7
• EATA	32.8	34.5	31.7	23.4	17.5	32.0	28.2	43.5	43.6	45.4	69.7	45.8	27.2	10.5	39.6	35.0
• COME	38.6	41.4	39.0	34.4	14.9	44.6	7.3	52.9	51.0	56.9	72.4	51.7	15.7	33.8	53.3	40.5
• DeYO	35.5	38.5	35.3	22.0	23.9	37.1	15.3	42.4	40.4	47.6	70.2	50.8	23.7	18.0	48.8	36.6
• ZeroSiam (ours)	44.0	45.4	45.2	34.7	39.0	46.3	46.0	53.9	51.3	57.8	72.1	55.0	51.7	50.3	54.6	<b>49.8</b>

Table C: Additional results of TTA under **LABEL SHIFTS** with **BATCH SIZE=1** w.r.t. **Accuracy(%)**.

Model+Method	Noise			Blur			Weather				Digital			Avg.		
	Gauss.	Shot	Impul.	Defoc.	Glass	Motion	Zoom	Snow	Frost	Fog	Brit.	Contr.	Elastic	Pixel	JPEG	
ResNet50-GN	18.0	19.8	17.9	19.8	11.4	21.4	24.9	40.4	47.3	33.6	69.3	36.3	18.6	28.4	52.3	30.6
• Tent	1.2	1.5	1.3	10.0	2.1	14.3	11.2	8.2	11.7	0.8	70.1	41.6	3.4	49.5	52.3	18.6
• SAR	23.4	26.5	23.8	18.3	15.4	28.4	29.5	44.3	44.5	31.6	72.3	44.5	14.9	46.8	56.1	34.7
• EATA	19.2	21.7	19.4	17.9	13.0	23.5	25.7	39.7	43.6	34.5	69.4	38.4	20.0	34.9	53.2	31.6
• COME	17.8	19.7	17.8	19.7	11.2	21.3	24.9	40.3	47.7	33.6	69.0	35.7	18.6	27.9	51.7	30.5
• DeYO	41.0	43.8	42.2	22.9	23.3	41.4	15.9	54.0	52.3	20.7	73.4	53.6	48.1	60.1	59.8	43.5
• ZeroSiam (ours)	40.3	42.4	40.5	32.6	33.2	41.2	44.3	53.6	53.1	59.5	72.7	52.1	46.8	58.7	58.7	<b>48.6</b>
ViT-Base	9.4	6.7	8.3	29.1	23.4	34.0	27.0	15.8	26.3	47.4	54.7	43.9	30.5	44.5	47.6	29.9
• Tent	29.2	7.9	21.1	49.3	46.9	53.7	47.5	18.0	19.2	63.7	71.1	61.4	51.8	63.6	62.2	44.4
• SAR	24.8	18.3	24.1	38.2	31.9	42.1	35.5	31.1	37.5	52.3	61.0	52.3	36.3	52.0	52.4	39.3
• EATA	30.7	26.8	31.3	42.9	39.5	47.8	35.6	38.0	43.7	60.2	65.8	57.7	46.9	59.4	58.0	45.6
• COME	51.1	47.9	52.5	57.2	58.0	63.1	60.5	67.3	64.8	72.8	77.6	67.6	67.4	73.4	69.8	<b>63.4</b>
• DeYO	53.2	36.2	54.5	58.2	59.3	64.3	41.8	68.6	66.7	73.8	78.3	67.4	69.3	74.1	71.0	62.4
• ZeroSiam (ours)	49.9	50.2	51.0	56.0	56.4	60.8	58.4	65.5	64.4	71.9	77.4	66.1	65.9	71.5	68.7	62.3
ViT-Small	2.0	2.0	1.5	24.2	17.1	30.3	22.0	9.5	19.2	37.9	44.4	30.1	24.8	38.2	41.0	22.9
• Tent	0.3	0.3	0.2	43.4	37.2	45.7	36.6	4.6	22.3	58.4	66.0	54.7	27.0	56.8	55.3	33.9
• SAR	2.2	2.3	1.7	34.5	26.0	39.2	27.4	19.7	32.1	45.0	53.7	43.4	31.9	44.2	45.9	29.9
• EATA	2.1	2.3	1.7	29.1	21.8	34.6	25.0	14.7	24.8	42.8	49.5	39.4	28.7	42.7	44.2	26.9
• COME	0.5	3.5	0.4	47.8	46.9	52.7	16.9	37.3	53.6	64.3	70.6	58.8	55.8	63.5	60.4	42.2
• DeYO	0.4	0.8	0.3	48.7	47.3	53.2	21.2	46.6	54.2	64.9	70.9	59.4	57.5	64.1	61.0	43.4
• ZeroSiam (ours)	23.7	23.6	25.0	46.0	44.9	49.6	46.8	50.8	52.8	62.7	69.1	56.8	54.8	61.1	58.7	<b>48.4</b>
ConvNeXt-Tiny	21.4	27.7	22.1	24.5	11.0	32.5	31.2	44.5	52.5	39.5	72.0	44.8	23.1	17.7	55.8	34.7
• Tent	18.2	24.8	26.0	24.4	4.3	34.0	29.1	41.8	46.3	42.4	73.2	51.8	18.2	10.4	56.9	33.5
• SAR	30.2	33.6	30.2	25.8	11.1	33.3	31.0	44.9	47.6	37.8	73.0	46.2	22.7	18.2	56.3	36.1
• EATA	24.0	28.9	24.5	24.7	11.2	32.5	31.0	44.6	51.4	39.7	72.1	45.9	23.2	18.0	55.8	35.2
• COME	41.4	43.4	41.3	37.3	2.4	44.7	18.4	56.4	55.7	61.1	75.3	59.6	11.0	44.3	61.2	43.6
• DeYO	36.9	39.4	37.0	29.2	3.2	37.7	14.8	51.6	47.6	5.4	74.0	55.8	8.3	23.3	58.0	34.8
• ZeroSiam (ours)	41.3	43.3	41.1	36.3	31.4	43.8	42.2	54.9	53.7	61.5	74.2	58.2	41.0	49.8	59.2	<b>48.8</b>
Swin-Tiny	26.6	27.9	22.8	21.7	13.2	2										

Table D: Detailed results of TTA on the **BLIND-SPOT SUBSET**, *i.e.*, Table 6 in the main paper.

Model+Method	Noise			Blur				Weather				Digital				Avg.
	Gauss.	Shot	Impul.	Defoc.	Glass	Motion	Zoom	Snow	Frost	Fog	Brit.	Contr.	Elastic	Pixel	JPEG	
ResNet50-GN	18.0	19.8	17.9	19.8	11.4	21.4	24.9	40.4	47.3	33.6	69.3	36.3	18.6	28.4	52.3	30.6
• Tent	0.2	0.2	0.2	10.5	2.3	5.8	2.3	1.6	2.3	0.2	63.3	16.7	0.5	48.3	46.8	13.4
• SAR	17.0	19.6	16.9	15.8	11.4	22.2	24.0	5.8	42.0	25.4	69.0	38.9	1.3	31.9	54.2	26.4
• EATA	18.6	21.2	18.6	15.6	13.4	22.7	24.4	37.1	38.8	33.2	67.8	41.6	19.1	47.1	53.0	31.5
• COME	18.0	19.8	17.9	19.8	11.3	21.4	24.9	40.4	47.3	33.6	69.2	36.2	18.6	28.3	52.2	30.6
• DeYO	0.4	0.6	0.4	7.9	0.2	28.1	1.6	5.5	7.1	0.1	71.2	47.8	1.3	59.7	51.4	18.9
• ZeroSiam (ours)	38.0	42.7	39.0	27.9	34.0	41.1	43.3	52.1	44.3	59.1	60.2	51.2	53.8	60.3	45.4	<b>46.2</b>
ViT-Base	9.5	6.7	8.2	29.0	23.4	33.9	27.1	15.9	26.5	47.2	54.7	44.1	30.5	44.5	47.8	29.9
• Tent	0.2	0.2	0.1	56.5	54.0	60.4	0.5	1.4	1.0	0.2	77.5	67.4	0.3	71.6	68.7	30.7
• SAR	42.2	7.1	43.9	55.3	51.3	59.4	54.0	19.7	47.6	71.5	77.4	67.1	19.4	71.3	67.8	50.3
• EATA	26.4	20.3	32.2	45.7	37.5	48.6	42.3	37.2	47.5	62.2	65.7	63.1	46.8	60.1	59.8	46.4
• COME	0.1	0.1	0.1	56.9	58.4	63.5	0.5	68.3	64.7	73.4	77.1	67.1	69.1	73.4	69.5	49.5
• DeYO	0.1	0.3	0.2	59.4	60.4	65.1	3.8	69.7	67.6	74.5	78.5	68.7	70.8	75.0	71.2	51.0
• ZeroSiam (ours)	52.6	53.2	53.4	57.7	58.6	63.4	61.7	67.8	66.5	73.8	78.2	67.8	69.2	73.7	70.2	<b>64.5</b>
ViT-Small	2.0	1.9	1.5	24.3	17.1	30.2	21.8	9.5	19.3	37.9	44.4	29.9	24.9	38.2	41.3	22.9
• Tent	0.1	0.2	0.1	44.6	36.6	45.6	33.2	1.3	16.5	59.5	68.0	56.5	0.5	58.2	56.2	31.8
• SAR	2.1	2.2	1.6	31.1	23.7	39.2	27.5	9.8	40.0	51.8	66.4	46.7	23.4	53.2	49.8	31.2
• EATA	2.2	2.2	1.6	28.4	20.3	33.2	24.2	11.8	23.0	44.8	51.4	47.4	28.3	45.4	45.6	27.3
• COME	0.1	2.6	0.1	47.3	48.0	52.4	0.2	31.2	55.6	65.0	71.7	59.5	0.4	64.4	60.6	37.3
• DeYO	0.1	0.3	0.1	49.4	48.9	54.0	0.5	45.9	56.3	66.2	72.3	60.6	58.6	65.5	61.9	42.7
• ZeroSiam (ours)	25.1	25.4	27.6	48.2	47.9	52.5	50.6	54.3	55.5	65.6	71.8	59.2	59.4	64.6	61.2	<b>51.3</b>
ConvNeXt-Tiny	21.3	27.7	22.0	24.5	10.6	32.3	30.9	44.6	52.4	39.6	72.3	44.5	23.4	17.6	55.6	34.6
• Tent	15.5	12.9	25.2	21.3	2.1	30.0	25.3	30.3	40.4	1.8	72.6	50.1	14.3	3.2	56.4	26.8
• SAR	24.3	30.2	24.8	24.7	10.7	32.5	30.6	42.9	50.1	37.1	72.7	45.1	21.8	17.7	55.7	34.7
• EATA	23.7	29.1	24.5	24.6	11.1	32.5	30.7	44.3	50.4	39.9	72.0	46.2	23.2	17.9	55.7	35.0
• COME	41.1	42.7	40.4	29.4	0.4	33.3	2.4	25.1	24.9	0.2	74.2	57.7	0.6	27.6	58.3	30.6
• DeYO	34.9	35.5	35.3	22.0	0.9	23.0	3.0	38.6	29.1	0.3	72.1	52.3	1.8	22.1	55.6	28.4
• ZeroSiam (ours)	42.4	44.9	42.5	37.2	33.9	45.5	44.5	56.3	53.3	64.4	73.7	60.5	44.7	56.3	58.5	<b>50.6</b>
Swin-Tiny	26.9	27.7	23.0	21.7	13.2	26.4	25.3	41.2	45.8	47.7	67.8	39.2	22.5	8.4	33.2	31.3
• Tent	0.2	0.4	0.1	14.0	5.9	7.2	5.0	9.6	8.9	2.6	67.7	16.1	1.4	0.3	34.4	11.6
• SAR	27.3	29.0	24.8	21.6	14.9	26.7	25.7	36.6	45.3	47.5	67.8	39.4	10.5	8.6	36.5	30.8
• EATA	27.9	29.0	25.3	20.7	14.6	28.4	25.7	40.1	40.7	47.4	68.1	40.8	23.6	9.2	33.8	31.7
• COME	38.1	41.3	42.0	26.2	0.5	10.8	0.5	10.3	8.0	10.2	72.8	52.0	0.1	0.5	55.1	24.6
• DeYO	0.2	0.1	0.2	13.8	6.4	11.4	3.7	11.6	16.9	4.3	70.2	44.4	3.7	0.4	47.1	15.6
• ZeroSiam (ours)	45.1	47.5	47.0	35.2	40.3	46.1	46.9	56.1	51.9	58.5	68.6	54.8	54.7	52.9	56.3	<b>50.8</b>

Table E: Detailed results of TTA under the **MILD SCENARIO**, *i.e.*, Table 7 in the main paper.

Model+Method	Noise			Blur				Weather				Digital				Avg.
	Gauss.	Shot	Impul.	Defoc.	Glass	Motion	Zoom	Snow	Frost	Fog	Brit.	Contr.	Elastic	Pixel	JPEG	
ResNet50-GN	18.0	19.8	17.9	19.8	11.4	21.4	24.9	40.4	47.3	33.6	69.3	36.3	18.6	28.4	52.3	30.6
• Tent	5.1	6.1	5.4	15.0	10.8	22.1	22.9	25.8	33.2	3.1	70.4	42.7	11.0	48.1	54.2	25.1
• SAR	28.5	31.4	29.7	18.7	19.5	30.2	30.1	43.3	43.7	7.0	70.8	44.0	19.0	48.8	55.2	34.7
• EATA	37.3	39.1	39.4	28.1	27.1	36.8	39.1	50.8	49.0	55.8	72.0	50.1	41.8	55.7	58.1	45.4
• COME	17.9	19.7	17.7	19.7	11.3	21.4	24.9	40.4	47.5	33.6	69.1	35.9	18.6	27.9	52.1	30.5
• DeYO	39.6	42.1	40.6	22.2	23.3	38.3	37.7	50.4	49.4	3.0	73.0	50.3	41.9	55.5	57.7	41.7
• ZeroSiam (ours)	40.5	42.4	41.7	31.4	31.8	40.8	44.4	53.5	53.3	59.1	72.9	51.5	47.4	58.9	58.8	<b>48.6</b>
ViT-Base	9.4	6.7	8.3	29.1	23.4	34.0	27.0	15.8	26.3	47.4	54.7	43.9	30.5	44.5	47.6	29.9
• Tent	42.4	1.4	43.3	52.2	47.6	55.4	49.9	19.7	18.1	66.1	74.9	64.7	52.5	66.8	64.1	47.9
• SAR	44.3	14.0	45.7	52.9	49.8	56.0	51.1	58.3	50.6	66.5	74.6	64.3	55.5	66.5	64.0	54.3
• EATA	49.7	49.4	51.3	55.9	55.5	60.5	57.8	63.4	63.0	70.4	76.0	67.0	64.7	69.3	67.9	61.5
• COME	50.9	51.6	52.1	56.9	57.4	62.2	59.2	66.1	64.3	72.5	77.4	67.9	66.3	72.4	69.2	<b>63.1</b>
• DeYO	52.9	53.1	53.8	58.2	58.6	63.0	40.2	67.4	65.7	73.2	78.0	68.0	67.7	73.1	69.8	62.8
• ZeroSiam (ours)	50.5	51.0	51.5	57.1	56.8	61.2	58.6	64.9	64.5	71.9	77.2	67.6	65.6	71.5	68.5	62.6
ViT-Small	2.0	2.0	1.5	24.2	17.1	30.3	22.0	9.5	19.2	37.9	44.4	30.1	24.8	38.2	41.0	22.9
• Tent	0.5	0.6	0.4	39.5	33.0	42.5	34.0	10.3	37.1	54.5	63.6	51.7	31.5	53.1	52.3	33.6
• SAR	1.4	2.1	1.1	40.8	34.9	43.2	35.5	16.3	41.8	54.7	63.7	51.8	38.5	53.4	52.5	35.4
• EATA	22.4	20.6	23.6	45.0	43.0	47.2	43.5	48.5	49.9	60.7	66.4	56.6	52.7	58.3	57.2	46.4
• COME	0.2	0.4	0.2	47.7	46.3	51.3	19.6	37.9	52.7	63.6	69.8	58.3	54.1	61.8	59.2	41.6
• DeYO	0.2	0.3	0.2	47.9	45.8	51.4	33.6	44.5	53.0	63.5	70.1	58.5	55.3	62.4	59.8	43.1
• ZeroSiam (ours)	23.8	23.4	25.2	47.6	46.0	50.6	48.1	51.9	53.3	63.2	69.9	58.1	55.7	61.8	59.4	<b>49.2</b>
ConvNext-Tiny	21.4	27.7	22.1	24.5	11.0	32.5	31.2	44.5	52.5	39.5	72.0	44.8	23.1	17.7	55.8	34.7
• Tent	30.8	33.6	32.0	24.7	7.5	33.6	30.0	43.7	47.3	43.6	72.9	49.5	21.5	19.3	56.3	36.4
• SAR	33.4	35.6	33.7	27.1	8.1	34.1	30.7	44.6	47.3	17.0	72.8	48.8	22.0	24.4	56.1	35.7
• EATA	35.3	37.4	35.8	31.0	20.7	37.1	33.7	48.5	49.1	51.3	73.2	53.0	29.5	31.3	56.6	41.6
• COME	40.4	42.6	40.4	36.2	2.3	43.2	23.4	54.6	54.2	58.1	75.1	58.6	10.6	44.7	59.9	43.0
• DeYO	36.3	39.0	36.4	29.1	2.7	37.1	19.6	50.1	48.3	4.8	73.8	54.9	8.6	23.7	57.4	34.8
• ZeroSiam (ours)	39.6	41.7	39.3	33.8	27.3	42.0	38.7	53.2	51.8	59.3	73.8	57.0	36.5	44.2	58.2	<b>46.4</b>
Swin-Tiny	26.6	27.9	22.8	21.7	13.2	26.5	25.4	41.0	45.8	47.7	67					

## E ADDITIONAL DISCUSSIONS

### E.1 ZEROSIAM’S EFFICACY BEYOND COLLAPSE PREVENTION

ZeroSiam regularizes test-time entropy minimization from favoring non-generalizable shortcuts (c.f. Section 3.2), thereby improving its performance even in cases when no collapse occurs. As shown in Figure B, Tent drastically reduces entropy and eventually closes it to zero by inflating the logit norms and aligning all logits toward a dominant mode. Despite the reduction of entropy, it does not involve meaningful learning, and Tent thus fails to improve the accuracy on the first 250 batches of samples, where such biased signals can further degrade performance during a prolonged adaptation, as shown in Figure B. In contrast, ZeroSiam maintains a stable logit norm and center dominance ratio during entropy minimization, which successfully enhances TTA efficacy beyond collapse prevention, as shown in Figure B (a). Moreover, from Figure B (d), ZeroSiam does not greedily minimize the entropy loss. Instead, ZeroSiam converges to a low but non-zero entropy loss, while still enabling consistent accuracy improvement, *i.e.*, from 250 to 750 batches as in Figure B (a). Such convergence toward non-zero loss is also aligned with Theory 1, which shows that ZeroSiam inherently defines a lower bound of  $h_{min}$  for entropy optimization, preventing the model from degenerating into collapsed constant one-hot outputs that trivially minimize (*i.e.*, zero out) the entropy loss.

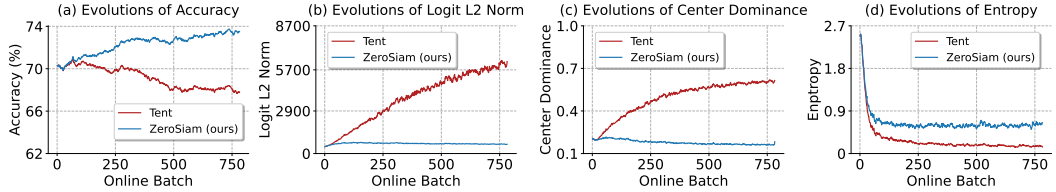


Figure B: Empirical evidence of ZeroSiam for boosting stability and efficacy. (a-d) record the ODD accuracy, logits  $L_2$  norm, center dominance, and entropy in model predictions under a mild test scenario (Wang et al., 2021). Experiments are run on ImageNet-C (Bright, level 5) with ViT-Base.

### E.2 EVOLUTIONS OF DIVERGENCE LOSS IN ZEROSIAM

We provide additional results of how the divergence loss evolves during adaptation. As shown in Figure C, the divergence loss increases more rapidly and substantially under a more imbalanced stream. Such a phenomenon is also aligned with changes of the predictor as shown in Figure 2 (a), where a larger divergence from an identity mapping results in a larger similarity loss. Overall, these results suggest *an adaptive regularization strength* according to the degree of collapse risk in the scenario, indicating the efficacy of our asymmetric entropy optimization design.

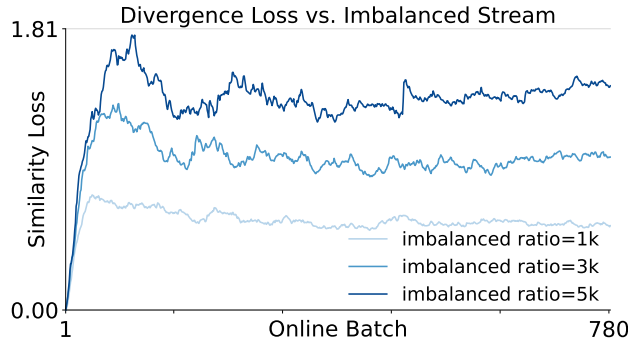


Figure C: The evolution of divergence loss during TTA. Results are reported on ImageNet-C (Snow, level 5) with ResNet50-GN under online streams with varying imbalanced ratios (Niu et al., 2023).

### E.3 ZEROSIAM FOR SAVING A COLLAPSED MODEL

Interestingly, we further demonstrate that ZeroSiam can sometimes save a model that has already collapsed. To illustrate this, we first run Tent on an imbalanced data stream until collapse occurs, and then apply ZeroSiam. As shown in Figure D, ZeroSiam helps restore strong accuracy after 300 batches of adaptation. This recovery is driven by the asymmetric alignment in ZeroSiam, which makes collapsed solutions no longer a stable minimum, encouraging the model to escape the collapsed mode and re-cluster samples. However, this does not fully explain how class-wise clusters that are consistent with pre-training re-emerge. We hypothesize this is because only the affine parameters in the normalization layers are updated during testing, which introduces a small adjustment to the model that makes performance recovery possible. Notably, we observe that the predictor in ZeroSiam has to be randomly initialized (*e.g.*,  $\theta_h = \mathbf{I} + 0.1 \mathbf{W}$ ,  $\mathbf{W} \sim \mathcal{N}(0, \mathbf{I})$ ) so as to derive from the identity and also remain learnable during TTA to enable the collapse recovering effects. Even so, recovery succeeds in only 4 out of 7 domains, suggesting that while promising, collapse recovery with ZeroSiam remains an open question, and we leave it for future work.

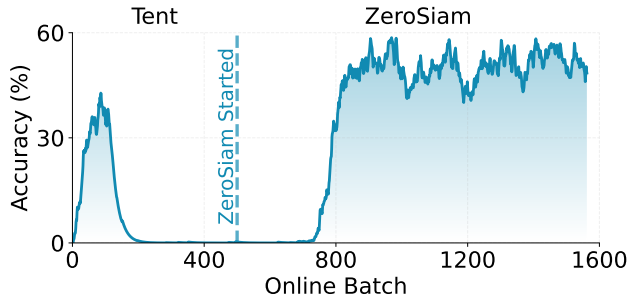


Figure D: Efficacy of ZeroSiam for saving a collapsed model. Results are reported on ImageNet-C (Shot, level 5) with ViT-Base under **ONLINE IMBALANCED LABEL SHIFTS** (imbalance ratio =  $\infty$ ).

### E.4 SENSITIVITY OF $\alpha$ IN ZEROSIAM

ZeroSiam introduces an efficient asymmetric architecture, with a self-training objective and a divergence alignment term, where  $\alpha$  balances the two objectives. Our architecture can be used across a wide range of objective combinations, as verified in Table 10, indicating our generality. In the main paper, we do not carefully tune  $\alpha$  for test-time entropy minimization. Instead, we adopt symmetric KL as the divergence and directly set  $\alpha = 1$ , which provides an elegant overall formulation of Eqn. (4) by  $H(p_o, \text{sg}[p_r]) + H(\text{sg}[p_r], p_o)$ . As verified in Table F, ZeroSiam consistently outperforms Tent with a wide range of  $\alpha$ , and achieves the best performance when  $\alpha \in [0.5, 1.5]$ .

Table F: Sensitivity of  $\alpha$  in ZeroSiam. We report **Accuracy (%)** on ImageNet-C (severity level 5) with ViT-Base under **ONLINE IMBALANCED LABEL SHIFTS**, where the imbalance ratio is  $\infty$ .

Method	No adapt	Tent	$\alpha = 0.5$	$\alpha = 1.0$	$\alpha = 1.5$	$\alpha = 2.0$	$\alpha = 2.5$	$\alpha = 3.0$
Accuracy (%)	29.9	47.3	63.9	64.1	63.9	63.3	62.4	61.0

### E.5 NECESSITY OF STOP-GRADIENT FOR ASYMMETRY

As verified in Theory 1, the online branch in ZeroSiam converges more rapidly towards the collapse solutions during TTA. The stop-gradient on the target branch prevents the target branch from also drifting toward the collapse modes, while providing a stable reference for the online branch. As shown in Table G, removing stop-gradient leads to severe collapse, *e.g.*, reducing the accuracy from 51.6%  $\rightarrow$  20.5% on ResNet50-GN. Similar results are also observed in SimSiam (Chen & He, 2021) and BYOL (Grill et al., 2020), underscoring stop-gradient as a key component in asymmetry.

Table G: Importance of stop-gradient operation. Results are reported on ImageNet-C (severity level 5) under **ONLINE IMBALANCED LABEL SHIFTS** (imbalance ratio =  $\infty$ ) regarding **Accuracy (%)**.

ResNet50-GN	Noise			Blur			Weather			Digital			Avg.			
	Gauss.	Shot	Impul.	Defoc.	Glass	Motion	Zoom	Snow	Frost	Fog	Brit.	Contr.	Elastic	Pixel	JPEG	
ZeroSiam (ours)	42.9	45.1	43.1	35.1	36.1	44.5	49.2	58.1	55.1	62.9	72.3	54.8	52.5	61.7	60.1	51.6
- w/o stop-grad	2.1	2.7	2.0	15.3	2.0	15.2	11.1	11.9	17.7	1.2	71.9	43.5	3.8	50.9	55.5	20.5
ViT-Base	Gauss.	Shot	Impul.	Defoc.	Glass	Motion	Zoom	Snow	Frost	Fog	Brit.	Contr.	Elastic	Pixel	JPEG	Avg.
ZeroSiam (ours)	52.3	52.6	53.4	57.7	58.7	62.7	61.1	67.6	66.0	73.3	78.0	67.0	67.9	73.5	70.1	64.1
- w/o stop-grad	2.8	0.8	12.8	54.1	51.1	57.6	33.7	6.3	8.0	68.7	76.1	65.9	4.4	69.2	66.3	38.5

## F MORE DISCUSSIONS WITH REINFORCEMENT LEARNING

Entropy collapse is also a common challenge within reinforcement learning, where policies can degenerate (*e.g.*, become deterministic and lose diversity) due to biased or noisy advantage estimation, insufficient exploration, reward hacking, or overly aggressive updates (Mnih et al., 2016; Haarnoja et al., 2018; Ahmed et al., 2019). To address this, trust-region methods such as TRPO (Schulman et al., 2015) and PPO (Schulman et al., 2017) constrain each update step in policy space through KL-divergence penalties or clipping, ensuring gradual and stable improvement. Similar principles appear in value-based methods (Mnih et al., 2015; Schwarzer et al., 2023; Nauman et al., 2024), where target networks provide a stable anchor to stabilize bootstrapped updates against rapidly changing estimates. These approaches share with ZeroSiam the key idea of structurally constraining updates to counter collapse. Specifically, ZeroSiam’s online branch with gradient updates resembles a fast-updating policy (*i.e.*, with extra updates in the predictor), while the stop-gradient target branch serves as an anchor, effectively forming a lightweight trust region in the entropy minimization landscape. This connection situates ZeroSiam as a general collapse-prevention mechanism, linking stabilization strategies across TTA, self-supervised learning, and reinforcement learning.